On the mechanism of dynamic response amplification of cable transport line: application to the design based on the cable tension signal analysis

Hugo Bécu, Claude-Henri Lamarque, Alireza Ture Savadkoohi

On the mechanism of dynamic response amplification of cable transport line: application to the design based on the cable tension signal analysis

Hugo Bécu[1], Claude-Henri Lamarque[2], and Alireza Ture Savadkoohi[3]

[1]Research engineer, PhD, University of Lyon, ENTPE, Ecole Centrale de Lyon, CNRS, LTDS, UMR5513, Vaulx-en-Velin, France. Email: hugo.becu@gadz.org

[2]Professor, PhD, University of Lyon, ENTPE, Ecole Centrale de Lyon, CNRS, LTDS, UMR5513, Vaulx-en-Velin, France. Email: claude.lamarque@entpe.fr

[3]Director of research, PhD, University of Lyon, ENTPE, Ecole Centrale de Lyon, CNRS, LTDS, UMR5513, Vaulx-en-Velin, France. Email: alireza.turesavadkoohi@entpe.fr

ABSTRACT

Cables are used for many engineering applications such as transport systems that involve mobile cables suspended between supports for carrying attached vehicles. Because of the inherent cable's flexibility and the modification of dynamics properties during movement, such systems are sensitive to self sustained oscillations under steady-state conditions. To provide an understanding of such vibratory excitation sources and a design method to prevent operating problems, this paper proposes a real case study of a chairlift and the development of an original model. The aim is to highlight the mechanisms responsible for the dynamic response amplification of the cable line. The method is based on a reduction of the complete dynamic model to a single mode which localises the vibration energy along the cable loop. The reduced model thus obtained takes the form of a Mathieu-Hill parametric excitation oscillator. The stability study reveals zones of instability in which the dynamic system response increases. The approach is then validated on the real case study by positioning the chairlift's operating points in the stability diagram according to different configurations. Operating points are determined using the signal of the evolution of the static tension of the cable during the

movement of the vehicles. Based on the case study, a general methodology for modifying design parameters is proposed to avoid undesirable line dynamics.

INTRODUCTION

Cable structures are involved in many engineering fields and applications like bridges, power lines, elevators, offshore platform, robots. Cable element have been the subject of numerous publications in the state of the art because of the multiplicity of models and possible simplifications to describe the mechanical behaviour in statics (Crussels-Girona et al. 2017; Bertrand et al. 2020) and dynamics (Saxon and Cahn 1953; Irvine 1992; Fei et al. 2020; Fei and Danhui 2020; Xu et al. 2022). Cables are flexible structure showing nonlinearities (Rega 2004; Berlioz and Lamarque 2005; Lacarbonara 2013; Bertrand et al. 2022) due to their slender geometrical characteristics (Marigo 2014). In this paper, the problem of a moving cable assembly is addressed with application to cable transport systems for which one cable in translation to move suspended masses. The cable transport applications' state of the art is fragmentary since the mechanical studies are generally restricted to a single cable span located between two supports where the cable is supposed to be embedded. Due to the couplings on the global scale of the system, a local approach limits the interpretation of the physical phenomena that the model is able to capture. Analytical works are mainly focused on statics equilibrium using approximate methods (Czitary 1962; Schneigert 1964). More recently, numerical models are generally restricted to the statics or dynamics study of a single cable at rest without translation effects (Portier 1984; Brownjohn 1998; Ntarladima and Gerstmayr 2023). (Renezeder et al. 2005; Hurel et al. 2018) studied a mobile cable by justifying a quasi-static approach due to a little increase of the sag observed at usual speed.

To the best of the author's knowledge, only few research studies have dealt with pumping oscillations affecting continuously moving cable transport lines. Pumping phenomenon is a strong vertical oscillation of the cable between two intermediary supports. Portier's (Portier 1985) work is based on the intuition that pumping oscillations can be explained by cable tension pulses introduced at the cable supports by vehicles crossing. Löscher's (Löscher 1997; Engel and Löscher 2005) explanation of pumping is based on a resonant interaction between periodically circulating loads and

the cable. Mode shape is assumed to be collinear with the static shape and oscillation amplitude calculation is performed using a numerical integration scheme on a grid of speed and inter-vehicle spacing parameters. Renezeder (Renezeder 2006; Renezeder et al. 2006) performs transient calculations on a single-cable transport system modeled by finite elements with a commercial software. Sag oscillations are interpreted as a linear resonance generated by an external excitation. According to an alternative approach, but with similar conclusions, Knawa (Knawa-Hawryszków 2017) characterizes the modes of a cable car line and explains pumping oscillations as a linear resonance with a dynamic perturbation generated by the periodic distribution of vehicles. Babaz's (Babaz 2016) applied research work focuses on the pumping oscillations of continuously moving cable as a nonlinear phenomenon.

The various works available in the literature do not provide a robust design methodology for anticipating the pumping phenomena and for quantifying the influence of design parameters such as static tension or cable speed. Therefore, this paper proposes an original explanation of the pumping oscillations based on a stability study the Mathieu-Hill equation derived from a reduced dynamic model. An application with a case study of a chairlift showing pumping is proposed.

Firstly, the pumping oscillation description is given in a general framework and a presentation of the studied cable transport system is made. Then, the experimental protocol used to trigger pumping oscillations of the real system is described and the influencing parameters are highlighted. In the light of these initial findings, a heuristic explanation is proposed for the mechanisms that cause pumping oscillations. Secondly, a mathematical modelling is made by writing the dynamic equations of the whole installation considering the overall cable loop and the coupling with system's subcomponents. A modal approach is used, based on the results of a previous work (Bécu et al. 2023; Bécu et al. 2024). Vibration modes are calculated accounting for interactions between the cable in translation at variable speed, the supports and the pulleys at the end stations of the installation, with a trace of cable geometric non-linearities through the inclusion of a static correction in the calculation. The mass of the vehicles is assumed to be uniformly distributed along the cable to obtain a model underlying the modal calculation that is homogeneous and does not vary over time.

CASE STUDY PRESENTATION AND PUMPING OSCILLATIONS

In this paper, the cable transport system under study is a chairlift composed of (Figure 1, Table 1):

- A closed loop of track and haul rope of length L [m]. A forward path links the bottom station to the top one, and a return path links the top station to the bottom one.
- Vehicles equidistantly spaced by a length a l_d [m]. Vehicles are connected, guided and pulled by the cable.
- Two pulleys in a roughly horizontal plane at both ends of the installation. Pulleys deflect the rope loop. The tension bullwheel at the bottom station ensures mechanical tensioning T [N] via a hydraulic circuit that activates a cylinder. The drive bullwheel at the top station sets the rope loop in motion and is connected to the electric drive.
- An electric motor, a gearbox and a transmission shaft linked to the pulley.
- Towers along the cable path. Intermediate supports maintain an acceptable distance between the cable line and the ground. Two types of support are used, depending on whether the cable is deflected through the support at a positive angle (compression tower) or a negative angle (support tower). The contact between the cable and the structure is made by a sheave assembly equipped with small-diameter pulleys known as rollers. The sheave assembly is an articulated structure that deforms according to the cable geometry.

Pumping is a well-known oscillating phenomenon in the ropeway industry. Cable spans are affected in the frequency range of $[0.1, 1]$ Hz with possible coupling of vehicle pendulum oscillations (Figure 2). Pumping starts and stops at steady-state rope speed V_0 [m/s] for small variations of:

- vehicle load m_v [kg] ;
- cable's speed V_0 [m/s] ;
- spacing l_d [m] between the N_v vehicles on the line.

Pumping is highly sensitive to design parameters such as the static tension T [N] imposed by the

hydraulic cylinder, or to operating parameters such as number of passenger and cable speed V_0 [m/s]. Pumping is undesirable for a number of reasons prompting manufacturers and operators to ensure that installations are not subject to it, particularly in the context of the development of urban applications of ropeways as a means of mass transit:

- Dynamic loading cycles cause premature fatigue in the mechanical components of the sheave assembly and tower structures ;
- Line clearance is reduced by the amplitude of the cable and vehicle dynamic displacement ;
- Discomfort and apprehension is induced on passengers.

The frequency range of pumping oscillations corresponds to the frequencies associated with motion sickness, which in some cases causes kinetosis.

EXPERIMENTAL PROTOCOL TO HIGHLIGHT THE PUMPING

A chairlift line affected by pumping is studied as application case. After several years in service, the passenger flow was increased by adding new vehicles on the cable loop. The number of vehicles increased from N_v^0 to N_v^1. The pumping then has appeared in a span at a specific operating speed V_0 [m/s] during pre-commissioning tests. In the absence of a tool able to predicting this dynamic behaviour in the design phase, and of any precise understanding of the mechanisms behind the activation of pumping, an experimental protocol was set up to empirically study the influence of control parameters (V_0, N_v) ([m/s],[ ]) to the activation and disappearance of pumping on the chairlift line.

The Table 2 summarizes the speed V_0 [m/s] and vehicle number N_v [ ] configurations tested with a description of oscillation observations in the cable span affected by pumping according to a color code (green: no oscillations, red: strong oscillations):

- Pumping oscillations occur predominantly for $V_0 = 4.25$ [m/s] with N_v^1 vehicle along the cable with:

- strong and high vertical amplitude oscillations of the cable are observed in the span 8 according to a period $\delta t_c \approx 4.8$ [s] ;
- one mode shape response with one antinode located at mid span ;
- a transverse swaying of the vehicles according to a period $\delta t_v \approx 2.4$ [s] ;
- cable oscillations in phase opposition between the two sides of the track ;
- torque oscillations $\Delta C = C_{max} - C_{min}$ [Nm] in the driving motor C located in the upper station. These torque oscillations reflect the coupling effects of the cable's vertical oscillations on its longitudinal movement which is reflected in speed variations at the driving pulley. Torque is measured via the motor current (DC motor). The driving motor is speed-controlled by a PID corrector integrated into the controller. It explains the disturbance introduced on the motor torque which is an image of the cable's dynamic disorder.

- By increasing the cable speed to 4.5 [m/s] and 5 [m/s], cable and vehicle oscillations gradually disappear (see color code in orange and green in Table 2), in the same way as the oscillations observed on the motor torque (see Table 2).
- Based on this observation, a vehicle was removed from the line such as $N_v = N_v^1 - 1$ [ ]. No dynamic disorder is observed on the line at any cable speed $V_0 \in [4.25, 5]$ [m/s]. Measurements have been made for only the cable speed $V_0 = 4.25$ [m/s] (see Table 2) which showed the absence of any noticeable oscillations in the cable and motor torque compared with the previously tested configuration.

HEURISTIC ANALYSIS OF THE PUMPING

Internal self-excitation

On continuous-motion cable transport system, the equidistant distribution of vehicles along the cable loop introduces a spatial period equal to the inter-vehicle distance $l_d = \frac{L_0}{N_v}$ [m]. When the cable is in steady state movement at a constant speed V_0 [m/s], the movement of vehicles seen from

a fixed point on the line is periodic with a passage frequency

$$f_e = \frac{V_0}{l_d} = \frac{\Omega}{2\pi}. \tag{1}$$

By changing the number of vehicles N_v [ ] on the line from a value of N_v^0 [ ] to N_v^1 [ ], the passage frequency is modified by a relative value

$$\Delta f_e = \frac{N_v^1 - N_v^0}{N_v^0}. \tag{2}$$

The static state of the cable line also depends on the position of the vehicles. The highly non-linear nature of the static cable line equilibrium problem introduces a strong dependence of the cable tension T_s [N] and sag values, with influence on the cable curvature κ, on the positions successively occupied by the vehicles (see Figure 3).

The problem can thus be reduced to a parametric dependence on a geometric parameter l_c [m] describing the set of geometric configurations occupied by the system over time at the origin of a source of periodic internal dynamic disturbance of fundamental frequency f_e [Hz] when the cable is in translational movement. In the case presented here, the Table 3 summarizes the excitation pulsation $\Omega_e = 2\pi f_e$ [rad/s] associated with each line configuration tested.

Geometric coincidence

On single-cable system, when a vehicle is close to an intermediate tower, the clamp that connects it to the cable comes into contact with a zone dedicated to ensuring smooth passage of the vehicle from one side of the support to the other. Technologically speaking, this zone is referred to as a sheave assembly and is made up of a set of small-diameter pulleys interconnected by beams linked by pivots. This local contact alters the force balance, producing a contact resultant $\underline{R}$ which is the sum of the surface contact pressures between the clamp jaws gripping the rope and the roller grooves of the rubber tyre. This contact force, which is absent when the vehicle is outside a support zone, modifies the value of the local cable tension and thus causes a local dynamic disturbance ΔT_s within the moving system at V_0 speed via the static tension T_s. The intensity of the tension disturbance

depends on the parameters governing the geometry of the support, the cable, the vehicle load $\underline{P}$ and the sheave assembly crossing kinematics. From the point of view of the standard, the centripetal acceleration caused by the geometry of a circle arc-length support of radius R [m] is regulated by the following criterion,

$$\frac{V_0^2}{R} < 2.5 \text{ m/s}^2, \tag{3}$$

which limits the dynamic component of the tension disturbance caused by the crossing trajectory.

When two vehicles pass simultaneously over the two adjacent supports that separate a cable span, the local dynamic tension disturbance ΔT_s in the cable is locally amplified by a cumulative effect resulting in a modified static tension T_s^+ (see Figure 4).

Cable line dynamics

From a dynamic point of view, the pumping oscillations of the cable loop with the vehicles can be dissociated from the dynamic response of the stations and the supports as the natural frequencies of these substructures are higher than those observed on the cable line. Under these assumptions, the dynamics of a cable transport line is described by the mechanical equations of the cable and the interface with other substructures. A model of a translating cable with an instantaneous speed V_0 and an acceleration A_{V_0} such as $\underline{V}_0 = V_0\ \underline{t}$, $\underline{A}_{V_0} = A_{V_0}\ \underline{A}_{V_0}/\|\underline{A}_{V_0}\|$ is proposed in (Bécu et al. 2023). The description is based on the cable dynamic displacement

$$\underline{U}(S,t) = u(S,t)\ \underline{t} + v(S,t)\ \underline{n} + w(S,t)\ \underline{e}_z, \tag{4}$$

expressed according to the curvilinear abscissa $S \in [0, L]$, with L the cable length, in the cable local frame $(\underline{t}, \underline{n}, \underline{e}_z)$ and given by the tangent vector $\underline{t}$, the normal vector $\underline{n}$ and the out of plane vector $\underline{e}_z$. Keeping only the linear contributions, it leads to the cable dynamic equations in three

spatial dimensions:

$$\begin{cases} \mu\ddot{u} + c_u\dot{u} + \frac{T_s}{\|\underline{X}'\|}\kappa\big(v' + \kappa u\big) - EA(u'' - \kappa v') - 2\mu V_0\dot{u}' + \mu V_0^2 u'' + \mu A_{V_0} u' &= 0, \\ \mu\ddot{v} + c_v\dot{v} - \frac{T_s}{\|\underline{X}'\|}(v'' + \kappa u') - \kappa EA(u' - \kappa v) - 2\mu V_0\dot{v}' + \mu V_0^2 v'' + \mu A_{V_0} v' &= 0, \\ \mu\ddot{w} + c_w\dot{w} - \frac{T_s}{\|\underline{X}'\|}w'' - 2\mu V_0\dot{w}' + \mu V_0^2 w'' + \mu A_{V_0} w' &= 0. \end{cases} \tag{5}$$

with c_u, c_v, c_w the damping coefficients, $T_s(S)$ the static cable tension and $\underline{X}(S)$ the static cable position, $\bullet'$ derivatives with respect to the curvilinear variable S and $\dot{\bullet}$ derivatives with respect to the time variable t.

A mode of vibration is defined as the small undamped in-phase oscillations of the structure around a static state, which may depend on a prestress load, given by a modal shape

$$\underline{\Phi}_k = \Phi_{uk}\ \underline{t} + \Phi_{vk}\ \underline{n} + \Phi_{wk}\ \underline{e}_z \tag{6}$$

and a modal frequency

$$f_k = \omega_k / 2\pi \tag{7}$$

such as the dynamic response is given by variable separation

$$\underline{U}(S,t) = q(t)\ \underline{\Phi}_k(S) = e^{j\omega_k t}\ \underline{\Phi}_k(S). \tag{8}$$

Under several conditions concerning the nature of the mechanical model - linear, time-independent, undamped, symmetric - forms a basis for the solution space of the underlying dynamic problem (spectral decomposition). Thus, any solution to the linear dynamics problem of a moving cable can be approximated by searching for the solution in a subspace spanned by a selection of modes $\left[\underline{\Phi}_k\right]$ obtained by solving the following modal problem without taking into account time-dependent

damping terms:

$$\left\{\begin{array}{rcl} -\omega_k^2\mu\Phi_{uk} + \frac{T_s(S)}{\|\underline{X}(S)'\|}\kappa\big(\Phi'_{vk} + \kappa\Phi_{uk}\big) - EA(\Phi''_{uk} - \kappa\Phi'_{vk}) + \mu V_0^2\Phi''_{uk} + \mu A_{V_0}\Phi'_{uk} &=& 0, \\ -\omega_k^2\mu\Phi_{vk} - \frac{T_s(S)}{\|\underline{X}(S)'\|}(\Phi''_{vk} + \kappa\Phi'_{uk}) - \kappa EA(\Phi'_{uk} - \kappa\Phi_{vk}) + \mu V_0^2\Phi''_{vk} + \mu A_{V_0}\Phi'_{vk} &=& 0, \\ -\omega_k^2\mu\Phi_{wk} - \frac{T_s}{\|\underline{X}(S)'\|}\Phi''_{wk} + \mu V_0^2\Phi''_{wk} + \mu A_{V_0}\Phi'_{wk} &=& 0. \end{array}\right. \tag{9}$$

Using a projection, a reduced order model (ROM) is obtained under the following form,

$$\ddot{q} + \Big(c_k + \Psi_k^1(V_0)\Big)\dot{q} + \Big(\omega_k^2 + \Psi_k^2(V_0, A_{V_0})\Big)q = 0. \tag{10}$$

The Appendix 1 provides details on how to obtain the reduced order model.

The avantage of such a reduced order model is that it contains the spatial dynamic information along the system, provided by the mode, in a scalar equation form according to one degree of freedom q.

Modal excitation

The reduced order model given by Eq. (10) describes the dynamic behaviour of the cable transport system when the mode (Φ_k, ω_k) is activated in a privileged way. The projection on one mode allows to describe system dynamics around resonance under the assumption of a low modal coupling.

In the absence of an external excitation term in the second member of Eq. (80), the dynamic excitation comes from the static tension T_s and static curvature κ evolution when the cable and the vehicles are moving. The tension $T_s(S, l_c)$ and curvature $\kappa(S, l_c)$ depend on the geometric evolution parameter l_c (see subsection 4) which is related to time $l_c = V_0 \times t$ and can be written as follows

$$T_s(S,t) =< T_s > (S) + \Delta T_s(S,t), \tag{11}$$

$$\kappa(S,t) =< \kappa > +\Delta\kappa(S,t). \tag{12}$$

In other words, Eq. (80) can be rewritten in the non-dimensional generic form of a Mathieu-type

equation (Nayfeh and Mook 1979) with a parametric excitation term $a(T)$,

$$\ddot{q} + c\dot{q} + \Big(\delta + a(T))\Big)q = 0. \tag{13}$$

with

$$T = \frac{2\pi V_0}{l_d}t, \tag{14}$$

$$c = \frac{1}{\Omega^2}\Big(c_k + \Psi_k^1\Big), \tag{15}$$

$$\delta = \frac{1}{\Omega^2}\Big(\omega_p^2\big(< T_s >, < \kappa > \big) + \Psi_k^2\Big), \tag{16}$$

$$a(T) = \frac{1}{\Omega^2}\omega_p^2\big(\Delta T_s(S,T), \Delta\kappa(S,T)\big). \tag{17}$$

In the following, such a model is used to study the ability of a distributed excitation at fondamental frequency $f = \omega/2\pi$ along the cable line applied in the curvilinear abscissa S_i to generate a vibration at an observation point S_o.

Modal excitability

The notion of transfer $H(\omega)$ is introduced in modal analysis and establishes the link between a dynamic harmonic excitation at ω pulsation applied to a structure via input

$$inp(S_i, \omega) = F(S_i)\ e^{j\omega t} \tag{18}$$

and the observed structure's linear response

$$obs(S_o, S_i, \omega) = \Phi_k(S_o)\ Q(S_i, \omega)\ e^{j\omega t} \tag{19}$$

according to the mode k such as

$$obs(S_o, S_i, \omega) = H(S_i, S_o, \omega) \times inp(S_i, \omega) \tag{20}$$

and

$$\Big(-\omega^2 + j\omega c_k + \omega_k^2 \Big) Q = \int_0^L \Phi_k(S)\ \delta(S - S_i)\ F(S)\ \mathrm{d}S \tag{21}$$

One can combine Eq. (20) and Eq. (21) to obtain

$$H(\omega) = \frac{\Phi_k(S_0)\Phi_k(S_i)}{-\omega^2 + j\omega c_k + \omega_k^2} \tag{22}$$

It reveals modal excitability e_k (Balmès et al. 2004; Balmès 2005) which is the evaluation of the transfer $|H(\omega)|$ at resonance $\omega = \omega_k$,

$$e_k = \frac{\Phi_k(S_0)\Phi_k(S_i)}{\omega_k c_k}, \tag{23}$$

as a product of the modal controllability term $\Phi_k(S_i)$ and the modal observability $\Phi_k(S_o)$ divided by the damping effect.

Because of the parametric nature of excitation in Eq. (13) via the coefficient $a(T)$ depending on the non-dimensional time T, the notion of transfer is lost here. An equivalent notion of modal controllability is introduced. In the following, only the disturbance generated by static tension $\Delta T_s(S,T)$ variations is taken into account. The static curvature κ is supposed to be time independent. Thus, the parametric excitation term of Eq. 80 can be written

$$a(T) = \frac{1}{\Omega^2 \displaystyle\int_0^L (\Phi_{uk}^2 + \Phi_{vk}^2 + \Phi_{wk}^2)\mu\ \mathrm{d}S} \int_0^L \frac{\Delta T_s(S,T)}{\|\underline{X}'\|} \left[\Phi_{uk}^2\kappa^2 + \Phi_{uk}\Phi'_{vk}\kappa - \Phi_{vk}\Phi'_{uk}\kappa - \Phi_{vk}\Phi''_{vk} - \Phi_{wk}\Phi''_{wk} \right] \mathrm{d}S. \tag{24}$$

Here, the concept of modal excitability is the ability of the static tension perturbation $\Delta T_s(S,T)$, depending on its spatial distribution, to activate a mode $\underline{\Phi}_k(S)$. From Eq. (24), the level of parametric excitation is given by the integral over the rope length $S \in [0, L]$ of the product of $\Delta T_s(S,T)$ and the quantity

$$\Phi_{uk}^2\kappa^2 + \Phi_{uk}\Phi'_{vk}\kappa - \Phi_{vk}\Phi'_{uk}\kappa - \Phi_{vk}\Phi''_{vk} - \Phi_{wk}\Phi''_{wk} \tag{25}$$

that only depends on the mode shape relative amplitude along the cable. Thus, the level of parametric excitation $a(T)$ is maximum for a mode that localises the vibratory energy over a span of the cable line where the tension perturbation is also maximum.

Modal amplification

In linear theory, modal amplification quantity

$$-\omega^2 + j\omega c_k + \omega_k^2 \tag{26}$$

is linked to the resonance phenomenon when the excitation pulsation ω is equal to the mode pulsation ω_k by minimizing the norm of the denominator in the transfer Eq. (22). Here parametric resonance is discussed in the case of Eq. (13) and an equivalent definition of modal amplification is given.

The special feature of Mathieu-type equations Eq. (13) is that a time-periodic excitation term $a(T)$ appears as a coefficient in the differential equation governing the system. The excitation is designated by parametric. Unlike systems with only an external excitation source $F(S_i)$ where a small amplitude does not produce a strong system response except near one of the system's modal frequencies f_k (primary resonance), a small parametric excitation can produce a large system response if the excitation source frequency f is close to twice one of the system's modal frequencies, such as (Nayfeh and Mook 1979)

$$f = 2f_k. \tag{27}$$

Melde (Minorsky 1945) was the first to demonstrate experimentally the phenomenon of parametric excitation, using a string stretched between a rigid support and excited longitudinally by the vibration of one arm of a tuning fork. For excitation in the longitudinal direction, he observed that, for certain combinations of string linear mass and tension, a strong oscillation is produced in the vertical direction, with a frequency equal to half the excitation frequency f. This is called parametric resonance which corresponds to zones of dynamic instability. More generally, this observation

applies to parametric resonance condition of order n such that

$$f = n f_k. \tag{28}$$

The driving parametric excitation amplitude required to reach the instability zone increases with the order of the parametric resonance.

Heuristic interpretation of the pumping

According to a heuristic approach, the pumping phenomenon affecting continuous-motion cable transport lines can be interpreted as the coupling of strong modal controllability, observability and amplification:

- The high modal controllability is due to a parametric excitation driven by the cable tension periodic variations generated by the vehicles as they travel. These variations can be amplified by a geometric coincidence of vehicle crossing over supports in a cable span for which the responding mode has a large relative amplitude with respect to the other points of the cable.
- The high modal observability is due to a responding mode shape that localizes vibrating energy in a specific span.
- The high modal amplification is caused by a dynamic instability driven by a parametric resonance depending on:
    - the spectral content of dynamic disturbance of fundamental frequency f ;
    - a mode of frequency f_k of the cable loop involved in strong modal controllability.

ANALYTICAL STUDY OF THE PUMPING

Stability analysis

In the first section, it was seen that a parametric instability can cause a dynamic amplification of the cable line response when a mode with an high modal controllability and high modal observability is activated.

A stability analysis of the Mathieu-type equation Eq. (13) governing the pumping oscillations is proposed under the effect of a periodic perturbation in tension. The assumption is made that the pumping oscillations evolve in a subspace correctly described by a single mode $(\underline{\Phi}_k, \omega_k)$ and that the dynamic perturbation is uniform and localised in a single span for $S \in [L_1, L_2]$ such as

$$\Delta T_s(S,T) = \begin{cases} \Delta T_s(T), & \forall L \in [L_1, L_2], \\ 0, & \forall L \in [0, L_1[\cup]L_2, L]. \end{cases} \tag{29}$$

The tension can be written into Fourier series,

$$\begin{aligned} \Delta T_s(T) = \sum_i \Delta T_{si}^c \cos(iT) + \Delta T_{si}^s \sin(iT) &= \sum_i |\Delta T_{si}| e^{j\psi_i} e^{jiT} + |\overline{\Delta T}_{si}| e^{-j\psi_i} e^{-jiT} \\ &= \sum_{i=-\infty}^{+\infty} |\Delta T_{si}| e^{j(iT+\psi_i)} = 2\sum_i |\Delta T_{si}| \cos i(T+\psi_i), \end{aligned} \tag{30}$$

with $\Delta T_{si}^c = 2|\Delta T_{si}|\cos(\psi_i)$, $\Delta T_{si}^s = -2|\Delta T_{si}|\sin(\psi_i)$. A parameter ϵ is introduced, such as

$$\epsilon = \frac{1}{\Omega^2}|\Delta T_s(T)| \frac{1}{\int_0^L (\Phi_{uk}^2 + \Phi_{vk}^2 + \Phi_{wk}^2)\mu \, \mathrm{d}S} \int_0^L \frac{1}{\|\underline{X}'\|} \left[\Phi_{uk}^2\kappa^2 + \Phi_{uk}\Phi_{vk}'\kappa - \Phi_{vk}\Phi_{uk}'\kappa - \Phi_{vk}\Phi_{vk}'' - \Phi_{wk}\Phi_{wk}'' \right] \mathrm{d}S, \tag{31}$$

where $|\Delta T_s(T)| = \frac{1}{\sqrt{2}} \sqrt{\sum_{i=1}^{\infty} (|\Delta T_{s_i}^c|^2 + |\Delta T_{s_i}^s|^2)}$. Without loss of generality, Eq. (13) can be rewritten in the following form,

$$\frac{\mathrm{d}^2 q(T)}{\mathrm{d}T^2} + \epsilon c \frac{\mathrm{d}q(T)}{\mathrm{d}T} + (\delta + \epsilon \Delta T^*(T)) q(T) = 0, \tag{32}$$

with $\Delta T^*(T) = \frac{\Delta T_s(T)}{|\Delta T_s(T)|}$.

Eq. (32) highlights a multi-harmonic $T_s^*(T)$ parametric excitation so that it is called Mathieu-Hill equation. In order to detect pumping, which corresponds to operation in an unstable zone where the response q is theoretically unbounded in the absence of non-linear and damping effects, a stability study of the Mathieu-Hill equation Eq. (32) is proposed using a multi-scale method.

Initially, no damping is taken into account on the cable line. It will then be added and modifications to the instability regions discussed.

The parametric excitation term is multi-harmonic,

$$\Delta T_s^*(T) = \sum_{i>0} \Delta T_{s_i}^{*c} \cos(iT) + \Delta T_{s_i}^{*s} \sin(iT). \tag{33}$$

The multi-scale method consists of developing the dynamic response $q(T)$ as a function of the parameter ϵ and time T (Nayfeh and Mook 1979):

$$T_i = \epsilon^i T, \qquad i \in \mathbf{N}, \tag{34}$$

$$\frac{\mathrm{d}}{\mathrm{d}T} = D_0 + \epsilon D_1 + \epsilon^2 D_2 + ..., \qquad \text{with } D_i = \frac{\partial}{\partial T_i}, \tag{35}$$

$$q(T) = q_0(T_0, T_1, T_2, ...) + \epsilon q_1(T_0, T_1, T_2, ...) + \epsilon^2 q_2(T_0, T_1, T_2, ...). \tag{36}$$

Developments at multiple scales are replaced in Eq. (32),

$$(D_0+\epsilon D_1+\epsilon^2 D_2+...)^2(q_0+\epsilon q_1+\epsilon^2 q_2+...)+\left[\delta+\epsilon\left(\sum_{i>0} \Delta T_{s_i}^{*c} \cos(iT)+\Delta T_{s_i}^{*s} \sin(iT)\right)\right](q_0+\epsilon q_1+\epsilon^2 q_2+...) = 0. \tag{37}$$

The terms at each order of Eq. (37) are identified.

At order ϵ^0, one can get:

$$D_0^2 q_0 + \delta q_0 = 0. \tag{38}$$

Thus, a solution q_0 is written:

$$q_0(T_0, T_1, T_2, ...) = Q(T_1, T_2, ...)\ e^{j\sqrt{\delta}T_0} + \overline{Q}(T_1, T_2, ...)\ e^{-j\sqrt{\delta}T_0}, \tag{39}$$

where Q does not depend on T_0.

At order ϵ^1, one can get:

$$D_0^2 q_1 + \delta q_1 = -2D_0 D_1 q_0 - \left(\sum_{i>0} \Delta T_{s_i}^{*c} \cos(iT) + \Delta T_{s_i}^{*s} \sin(iT) \right) q_0. \tag{40}$$

Resonance of order n is studied, $n \approx \sqrt{\delta} \rightarrow n = \sqrt{\delta} + \epsilon\sigma$, with σ a detuning parameter. By replacing q_0 by its expression given by the development to order ϵ^0, the terms of the second member of Eq. (40) are expressed and given by the Appendix 2.

In the dynamic equation at order ϵ, terms of the form $\mathcal{A}e^{j\sqrt{\delta}T_0}$ are resonant terms, i.e. if they are not zero, $\mathcal{A}(T_1, T_2, ...) = 0$, the solution q_1 is not bounded. However, we're looking for periodic solutions according to Floquet's theory, i.e. bounded solutions. $\mathcal{A}$ must therefore be zero: we say that we're eliminating the secular terms.

The resonant terms of the second member are of the kind $e^{j\sqrt{\delta}T_0}$ and are identified as

$$-2D_1 Q j\sqrt{\delta}\ e^{j\sqrt{\delta}T_0} - \Delta T_{s_{2n}}^* \overline{Q}\ e^{j(2n-\sqrt{\delta})T_0}. \tag{41}$$

because for $i = 2n = 2\sqrt{\delta} + 2\epsilon\sigma$:

$$e^{j(2n-\sqrt{\delta})T_0} = e^{j(2\sqrt{\delta}+2\epsilon\sigma-\sqrt{\delta})T_0} = e^{j2\epsilon\sigma T_0}\ e^{j\sqrt{\delta}T_0}.$$

Identifying $T_1 = \epsilon T_0$, cancelling the resonant terms of Eq. (41) leads to:

$$-2D_1 Q j\sqrt{\delta} - \Delta T_{s_{2n}}^* \overline{Q}\ e^{j2\sigma T_1} = 0. \tag{42}$$

The remaining non-resonant terms are:

$$\sum_i \Delta T_{s_i}^* Q\ e^{j(i+\sqrt{\delta})T_0} + \sum_{i\neq 2n} \Delta T_{s_i}^* \overline{Q}\ e^{j(i-\sqrt{\delta})T_0} + cc, \tag{43}$$

with cc the complex conjugate.

The particular solution in q_1 is calculated by keeping the non-resonant terms in the second

member of Eq. (40),

$$D_0^2 q_1 + \delta q_1 = -\sum_i \Delta T_{s_i}^* Q \; e^{j(i+\sqrt{\delta})T_0} - \sum_{i\neq 2n} \Delta T_{s_i}^* \overline{Q} \; e^{j(i-\sqrt{\delta})T_0} + cc. \tag{44}$$

q_1 is sought in the form:

$$q_1(T_0, T_1, T_2, ...) = \sum_i K_{1i}(T_1, T_2, ...) \; e^{j(i+\sqrt{\delta})T_0} + \sum_{i\neq 2n} K_{2i}(T_1, T_2, ...) \; e^{j(i-\sqrt{\delta})T_0}. \tag{45}$$

By substituting,

$$\begin{aligned} \sum_i K_{1i}(-(i+\sqrt{\delta})^2 + \delta) \; e^{j(i+\sqrt{\delta})T_0} + \sum_{i\neq 2n} K_{2i}(-(i-\sqrt{\delta})^2 + \delta) \; e^{j(i-\sqrt{\delta})T_0} + cc \\ = -\sum_i \Delta T_{s_i}^* Q \; e^{j(i+\sqrt{\delta})T_0} - \sum_{i\neq 2n} \Delta T_{s_i}^* \overline{Q} \; e^{j(i-\sqrt{\delta})T_0} + cc. \end{aligned} \tag{46}$$

By identification, $K_{1i} = \frac{\Delta T_{s_i}^* Q}{i(i+2\sqrt{\delta})}$, $K_{2i} = \frac{\Delta T_{s_i}^* \overline{Q}}{i(i-2\sqrt{\delta})}$. As,

$$q_1(T_0, T_1, T_2, ...) = \sum_i \frac{\Delta T_{s_i}^* Q}{i(i+2\sqrt{\delta})} \; e^{j(i+\sqrt{\delta})T_0} + \sum_{i\neq 2n} \frac{\Delta T_{s_i}^* \overline{Q}}{i(i-2\sqrt{\delta})} \; e^{j(i-\sqrt{\delta})T_0} + cc, \tag{47}$$

at order ϵ^2, one can get:

$$D_0^2 q_2 + \delta q_2 = -2D_0 D_2 q_0 - D_1^2 q_0 - 2D_0 D_1 q_1 - \left(\sum_i \Delta T_{s_i}^* \; e^{jiT_0} + \overline{\Delta T_{s_i}^*} \; e^{-jiT_0} \right) q_1. \tag{48}$$

The same procedure is applied to the order ϵ^2 and is given by the Appendix 3.

Finally, one can obtain the following equation by eliminating the secular terms at the order ϵ^2:

$$\begin{aligned} -2j\sqrt{\delta} D_2 Q + \frac{\Delta T_{s_{2n}}^* \sigma \overline{Q}}{\sqrt{\delta}} e^{j2\sigma T_1} - \left(\sum_{m\neq 2n} \frac{\Delta T_{s_m}^* \overline{\Delta T_{s_m}^*}}{m(m-2\sqrt{\delta})} + \sum_m \frac{\Delta T_{s_m}^* \overline{\Delta T_{s_m}^*}}{m(m+2\sqrt{\delta})} + \frac{\Delta T_{s_{2n}}^* \overline{\Delta T_{s_{2n}}^*}}{4\delta} \right) Q \\ - \left(\frac{\Delta T_{s_n}^{*2}}{n(n-2\sqrt{\delta})} + \sum_m \sum_{\substack{l \\ m-l=2n}} \frac{\Delta T_{s_m}^* \overline{\Delta T_{s_l}^*}}{l(l+2\sqrt{\delta})} + \sum_m \sum_{\substack{l \\ l\neq 2n \\ -m+l=2n}} \frac{\overline{\Delta T_{s_m}^*} \Delta T_{s_l}^*}{l(l-2\sqrt{\delta})} \right) \overline{Q} e^{j2\epsilon\sigma T_0} \end{aligned}$$

$$= 0. \quad (49)$$

The complex quantity $\Delta T_{s\,2n}^{*}$ is expressed as a function of its phase and modulus,

$$\Delta T_{s\,2n}^{*} = |\Delta T_{s\,2n}^{*}|\ e^{j\phi_1}. \quad (50)$$

The real term resulting from parametric excitation is denoted by

$$\Gamma_1 = \sum_{m\neq 2n} \frac{\Delta T_{s\,m}^{*}\overline{\Delta T_{s\,m}^{*}}}{m(m-2\sqrt{\delta})} + \sum_{m} \frac{\Delta T_{s\,m}^{*}\overline{\Delta T_{s\,m}^{*}}}{m(m+2\sqrt{\delta})} + \frac{\Delta T_{s\,2n}^{*}\overline{\Delta T_{s\,2n}^{*}}}{4\delta}, \qquad \Gamma_1 \in \mathbf{R}. \quad (51)$$

The complex term resulting from parametric excitation is denoted by

$$\Gamma_{2R} + j\Gamma_{2I} = |\Gamma_2|\ e^{j\phi_2} = \frac{\Delta T_{s\,n}^{*\,2}}{n(n-2\sqrt{\delta})} + \sum_{m} \sum_{\substack{l \\ m-l=2n}} \frac{\Delta T_{s\,m}^{*}\overline{\Delta T_{s\,l}^{*}}}{l(l+2\sqrt{\delta})} + \sum_{m} \sum_{\substack{l \\ l\neq 2n \\ -m+l=2n}} \frac{\overline{\Delta T_{s\,m}^{*}}\Delta T_{s\,l}^{*}}{l(l-2\sqrt{\delta})}. \quad (52)$$

The secular terms vanishing condition to be imposed for finding non-trivial solutions is given by Eq. (94) that can be rewritten according to Γ_1 and Γ_2,

$$-2j\sqrt{\delta}D_2 Q + \frac{|\Delta T_{s\,2n}^{*}|\sigma\overline{Q}}{\sqrt{\delta}} e^{j(2\sigma T_1+\phi_1)} - \Gamma_1 Q - |\Gamma_2|\overline{Q}e^{j(2\epsilon\sigma T_0+\phi_2)} = 0. \quad (53)$$

The two cancellation conditions for secular terms of orders ϵ and ϵ^2 given by Eq. (42) and Eq. (53) result from the expansion to different orders ϵ^n of a reconstituted modulation equation (Luongo et al. 2002):

$$-2j\sqrt{\delta}\ \frac{\mathrm{d}Q}{\mathrm{d}T} + \epsilon\left(-1 + \frac{\epsilon\sigma}{\sqrt{\delta}}\right)\overline{Q}|\Delta T_{s\,2n}^{*}|e^{j(2\sigma\epsilon T+\phi_1)} - \epsilon^2\left(\Gamma_1 Q + |\Gamma_2|\overline{Q}e^{j(2\epsilon\sigma T+\phi_2)}\right) = 0. \quad (54)$$

In order to eliminate the time T, the solution is sought in the form $Q = (Q_R + jQ_I)\ e^{j(\epsilon\sigma T+\frac{\phi_1}{2})}$, i.e. by injecting into Eq. (54),

$$-2j\sqrt{\delta}\left(\left[\frac{\mathrm{d}Q_R}{\mathrm{d}T}+j\frac{\mathrm{d}Q_I}{\mathrm{d}T}\right]e^{j(\epsilon\sigma T+\frac{\phi_1}{2})}+(Q_R+jQ_I)j\epsilon\sigma\ e^{j(\epsilon\sigma T+\frac{\phi_1}{2})}\right)+\epsilon\left(-1+\frac{\epsilon\sigma}{\sqrt{\delta}}\right)|\Delta T_{s2n}^*|(Q_R-jQ_I)\ e^{j(\epsilon\sigma T+\frac{\phi_1}{2})}$$
$$-\epsilon^2\left(\Gamma_1(Q_R+jQ_I)e^{j(\epsilon\sigma T+\frac{\phi_1}{2})}+(\Gamma_{2R}+j\Gamma_{2I})(Q_R-jQ_I)e^{j(\epsilon\sigma T+\frac{\phi_1}{2})}\right)=0. \quad (55)$$

The Appendix 4 gives details of how to obtain the conditions to guarantee the existence of a non-trivial solution of the kind $(Q_R, Q_I) = (q_R, q_I)\ e^{\gamma T}$. A polynomial of degree two in γ is obtained such that the solutions are written in the form,

$$\gamma_{1,2} = \frac{4\sqrt{\delta}\epsilon^2\Gamma_{2I} \pm \sqrt{16\delta C}}{8\delta}, \quad (56)$$

where $C = \epsilon^2\left[-|\Delta T_{s2n}^*|+2\sqrt{\delta}\sigma+\frac{\epsilon\sigma|\Delta T_{s2n}^*|}{\sqrt{\delta}}-\epsilon(\Gamma_1+\Gamma_{2R})\right]\left[-|\Delta T_{s2n}^*|-2\sqrt{\delta}\sigma+\frac{\epsilon\sigma|\Delta T_{s2n}^*|}{\sqrt{\delta}}+\epsilon(\Gamma_1+\Gamma_{2R})\right]$.

According to the Floquet theory, motion is at the boundary of the instability zone when $\gamma = 0$, i.e.:

$$\epsilon^2\Gamma_{2I} \pm \sqrt{C} = 0, \quad (57)$$

$$\epsilon^4\Gamma_{2I}^2 = C. \quad (58)$$

After further development by replacing the expression of C in Eq. (58), the equation to be solved is:

$$\epsilon^2|\Delta T_{s2n}^*|^2 - 4\delta\sigma^2\epsilon^2 - 4\sqrt{\delta}\sigma\epsilon^3(\Gamma_1+\Gamma_{2R}) + \frac{\epsilon^4\sigma^2}{\delta} - \epsilon^4(\Gamma_1+\Gamma_{2R})^2 + \epsilon^4\Gamma_{2I}^2 = 0. \quad (59)$$

Only quantities that imply a product between σ and ϵ with ϵ of order lower than two are considered, so Eq. (59) is written:

$$\epsilon^2|\Delta T_{s2n}^*|^2 - 4\delta\sigma^2\epsilon^2 - \epsilon^4(\Gamma_1+\Gamma_{2R})^2 + \epsilon^4\Gamma_{2I}^2 = 0. \quad (60)$$

One can obtain:

$$\sigma^2 = \frac{|\Delta T_{s2n}^*|^2}{4\delta} + \frac{\epsilon^2}{4\delta}\left[(\Gamma_1+\Gamma_{2R})^2 + \Gamma_{2I}^2\right]. \quad (61)$$

An expansion of σ is sought in the form $\sigma = k_1 + \epsilon k_2$, i.e.:

$$\sigma^2 = k_1^2 + 2\epsilon k_1 k_2 + \epsilon^2 k_2^2. \tag{62}$$

By identification with Eq. (61):

$$k_1 = \pm \frac{|\Delta T_{s_{2n}}^*|}{2\sqrt{\delta}}, \tag{63}$$

$$k_2 = \pm \frac{\sqrt{(\Gamma_1 + \Gamma_{2R})^2 + \Gamma_{2I}^2}}{2\sqrt{\delta}}. \tag{64}$$

Thus, the instability zones of the cable transport line dynamic response are given by:

$$\sigma > -\frac{|\Delta T_{s_{2n}}^*|}{2\sqrt{\delta}} - \epsilon \frac{\sqrt{(\Gamma_1 + \Gamma_{2R})^2 + \Gamma_{2I}^2}}{2\sqrt{\delta}}, \tag{65}$$

$$\sigma < \frac{|\Delta T_{s_{2n}}^*|}{2\sqrt{\delta}} - \epsilon \frac{\sqrt{(\Gamma_1 + \Gamma_{2R})^2 + \Gamma_{2I}^2}}{2\sqrt{\delta}}. \tag{66}$$

Note that $n = \sqrt{\delta} + \epsilon\sigma$, so $n^2 = \delta + 2\sqrt{\delta}\epsilon\sigma + \epsilon\sigma^2$. The boundaries separating zones of stability from zones of instability are expressed as a function of n and δ,

$$n^2 = \delta + \epsilon\left(2\sqrt{\delta}\left[- \frac{|\Delta T_{s_{2n}}^*|}{2\sqrt{\delta}} - \epsilon \frac{\sqrt{(\Gamma_1 + \Gamma_{2R})^2 + \Gamma_{2I}^2}}{2\sqrt{\delta}} \right]\right), \tag{67}$$

$$n^2 = \delta + \epsilon\left(2\sqrt{\delta}\left[\frac{|\Delta T_{s_{2n}}^*|}{2\sqrt{\delta}} - \epsilon \frac{\sqrt{(\Gamma_1 + \Gamma_{2R})^2 + \Gamma_{2I}^2}}{2\sqrt{\delta}} \right]\right). \tag{68}$$

After simplification, by replacing δ by its expression as a function of ω_p, the pulsation of the mode, and Ω, the fundamental of the parametric excitation,

$$n^2 = \frac{\omega_p^2}{\Omega^2} - \epsilon|\Delta T_{s_{2n}}^*| - \epsilon^2\sqrt{(\Gamma_1 + \Gamma_{2R})^2 + \Gamma_{2I}^2}, \tag{69}$$

$$n^2 = \frac{\omega_p^2}{\Omega^2} + \epsilon|\Delta T_{s2n}^*| - \epsilon^2\sqrt{(\Gamma_1 + \Gamma_{2R})^2 + \Gamma_{2I}^2}. \tag{70}$$

Up to now, damping has not been taken into account in stability study. A physical system always has damping, so it is reasonable to study the effect of a damping contribution $c\dot{q}$, reduced to the order ϵ, on the stability zones of the Mathieu-Hill equation Eq. (32),

$$\frac{\mathrm{d}^2 q(T)}{\mathrm{d}T^2} + \epsilon c\frac{\mathrm{d}q(T)}{\mathrm{d}T} + \Big(\delta + \epsilon\Delta T_s^*(T)\Big)q(T) = \epsilon f^*(T). \tag{71}$$

Details of developments with damping are given in the Appendix 5.

The boundaries separating zones of stability from zones of instability are expressed as a function of n et $\delta = \frac{\omega_p}{\Omega}$,

$$n^2 = \frac{\omega_p^2}{\Omega^2} - \epsilon\sqrt{|\Delta T_{s2n}^*|^2 - c^2n^2} - \epsilon^2\sqrt{\left(\Gamma_1 - \frac{c^2}{4} + \Gamma_{2R}\right)^2 + \Gamma_{2I}^2}, \tag{72}$$

$$n^2 = \frac{\omega_p^2}{\Omega^2} + \epsilon\sqrt{|\Delta T_{s2n}^*|^2 - c^2n^2} - \epsilon^2\sqrt{\left(\Gamma_1 - \frac{c^2}{4} + \Gamma_{2R}\right)^2 + \Gamma_{2I}^2}. \tag{73}$$

Assuming $c_0 = \epsilon c$,

$$n^2 = \frac{\omega_p^2}{\Omega^2} - \sqrt{\epsilon^2|\Delta T_{s2n}^*|^2 - c_0^2n^2} - \epsilon^2\sqrt{\left(\Gamma_1 - \frac{c_0^2}{4\epsilon^2} + \Gamma_{2R}\right)^2 + \Gamma_{2I}^2}, \tag{74}$$

$$n^2 = \frac{\omega_p^2}{\Omega^2} + \sqrt{\epsilon^2|\Delta T_{s2n}^*|^2 - c_0^2n^2} - \epsilon^2\sqrt{\left(\Gamma_1 - \frac{c_0^2}{4\epsilon^2} + \Gamma_{2R}\right)^2 + \Gamma_{2I}^2}. \tag{75}$$

Given the frequencies commonly involved in cable transport line oscillations, and the feedback from practical pumping situations which occur at a frequency equal to twice the frequency at which vehicles pass through the spans, $n = 2$ is adopted in the general case. Instability zones are therefore plotted around $\delta = n^2 = 4$ in Figure 5 for two excitation levels $|\Delta T_{s2n}^*|$ and three damping values c_0.

According to Figure 5, increasing damping has the effect of lifting the instability zone off the

δ axis and narrowing its width. Still according to Figure 5, the term $|\Delta T_{s_{2n}}^*|$, which represents the relative amplitude of the second harmonic of the parametric excitation by the tension ΔT_s^*, plays an important role in defining the instability zone: an increase in $|\Delta T_{s_{2n}}^*|$ widens the instability zone.

Analytical interpretation of the pumping

According to an analytical approach, the pumping phenomenon affecting continuous-motion cable transport lines can be interpreted as the consequence of a parametric resonance of the rope loop introduced by the quasi-static tension variations generated by the vehicles translation. Parametric resonance corresponds to the cable transport line's operating point associated with a zone of instability in the underlying dynamical system governing its behavior. As highlighted in **??**, the stability study can be reduced to the positioning of a point in the space of two reduced parameters (δ, ϵ) depending on the physical quantities of the cable transport line. Depending on the position of the operating point relative to the boundary, it is possible to define whether oscillations are likely to be amplified or not. The boundary is given by a plane curve separating a stable zone, for which the cable transport line motion is bounded, from an unstable zone, for which the cable transport line motion is theoretically unbounded. In this way, pumping results in a parametric instability phenomenon that leads to high-amplitude oscillations.

NUMERICAL VALIDATION AND DESIGN APPLICATION

Pumping mode

Using numerical data from the Table 1 corresponding to the chairlift case study and pumping observations, the first four vibration modes of the line are calculated numerically using an analytical-numerical method described by (Bécu et al. 2023; Bécu et al. 2024) (see Figure 6). The modes couple longitudinal and vertical dynamic of the rope. According to Figure 6, modes at $\omega_1 = 1.36$ [rad/s] and $\omega_3 = 1.75$ [rad/s] imply an anti-symmetrical vertical vibration between the two tracks, localised in certain spans, predominating over the longitudinal vibration, which is symmetrical. According to Figure 6,, modes at $\omega_2 = 1.41$ [rad/s] and $\omega_4 = 1.78$ [rad/s] imply a generalized longitudinal vibration over the entire line, outweighing the vertical vibration localised in certain

spans. According to Figure 6, modes at $\omega_2 = 1.41$ [rad/s] and $\omega_4 = 1.78$ [rad/s] lose all symmetry due to the different boundary conditions at the two end stations and translational effect of the cable, which are mainly involved in the longitudinal component of the dynamics, introducing a break in symmetry between the two tracks.

The mode at $\omega_1 = 1.36$ [rad/s] is identified as the pumping mode observed experimentally for $(V_0, N_v) = (4.25, N_v^1)$ configuration. In fact, this mode localises the energy of the vibration on both tracks in span 8, with a phase opposition of the oscillations between the two sides (see Figure 7). The modal properties actually display a dependence on the position of the vehicles over a period of travel T. A parametric study carried out with a model that takes into account the punctual nature of vehicle loading on the cable line shows that variations in modal pulsation are of the order of magnitude of $\Delta\omega_1 \approx 0.01\omega_1$.

Tension signal

The signal corresponding to the evolution of the quasi-static tension of the cable line at span # 8 is calculated numerically with a quasi-static model of the chairlift line. Numerical data used for the calculation come from the Table 1. The calculation is performed according to two configurations.

Firstly, for $(V_0, N_v) = (4.25, N_v^1)$, which corresponds to the pumping experimental configuration.

Figure 8 shows the evolution of the quasi-static tension T_s in span # 8 as a function of the evolution parameter l_c according to two models with $N_v = N_v^1$. Figure 8 curve in blue is based on a model that considers the tower support as a point. Figure 8 curve in yellow considers the support to be linear and the modification of the vehicle's equilibrium, by contact forces in addition to the effects of the tension, when it is in contact with the tower's sheave assembly. The effect of the interaction between the vehicle grip attached to the cable and the rollers of the sheave assembly can be observed for $l_c \in [22, 26]$ [m] with a transient cable tension decrease. That can be explained by a mechanism of force transfer: a part of the vehicle's weight, which was transmitted to the cable by the tension, is taken up by the support, reducing the corresponding tension value. This last model provides a more realistic description.

Figure 9 shows the relationship between the amplitude of the quasi-static tension perturbation and the quasi-static tension averaged over a period of vehicle travel in each of the two previous models with $N_v = N_v^1$. One can note that by considering the contact between the support and the vehicle in the underlying model, the variation in cable tension is amplified as the vehicles pass over the support. For the span # 8, the relative tension perturbation increases by 2.5 % to 5 %. This increase is explained by the geometrical coincidence effect, described in 4, in the span # 8 with the inter-vehicle spacing corresponding to $N_v = N_v^1$ and which involves contact forces. In this specific case, contact between vehicle and tower is an important factor in characterizing the excitation source.

Figure 10 shows the Fourier's transform of the tension signal over a period of vehicles passing through span # 8 with $N_v = N_v^1$. The left-hand plot shows the transform of the tension signal without considering the support contact. The right-hand plot is obtained from the tension signal with support contact taken into account. The effect of contact is to increase the amplitude of the peaks visible in the spectrum from the second harmonic.

Secondly, the same plots are made for the $(V_0, N_v) = (4.25, N_v^1 - 1)$ configuration for which pumping oscillations are no longer observed experimentally.

Figure 11 curve in blue is based on a model that considers the tower support as a point. Figure 11 curve in yellow considers the support to be linear and the modification of the vehicle's equilibrium by contact. The effect of the interaction between the vehicle grip attached to the cable and the rollers of the sheave assembly can not be longer observed for $N_v = N_v^1 - 1$ since there is no longer any geometric coincidence effect in the span # 8.

Figure 12 shows the relationship between the amplitude of the quasi-static tension perturbation and the quasi-static tension averaged over a period of vehicle travel in each of the two previous models with $N_v = N_v^1 - 1$. One can note that there is no longer any significant difference between the two calculation models. For the span # 8, the relative tension perturbation is 1.6 % without considering contact and 1.4 % by considering contact.

Figure 13 shows the Fourier's transform of the tension signal over a period of vehicles passing

through span # 8 with $N_v = N_v^1 - 1$. The left-hand plot shows the transform of the tension signal without considering the support contact. The right-hand plot is obtained from the tension signal with support contact taken into account. The effect of contact does not significantly modify the amplitude of the peaks visible in the spectrum.

Operating point positioning

The operating points (δ, ϵ) are calculated from the quasi-static tension signal analysis and the modal calculation corresponding to the two configurations $(V_0, N_v) = (4.25, N_v^1)$ and $(V_0, N_v) = (4.25, N_v^1 - 1)$. These points are placed in the stability diagram given by Figure 14 associated with the reduced model describing the chairlift's dynamic behavior:

- for $(V_0, N_v) = (4.25, N_v^1)$, which corresponds to the pumping experimental configuration:
    - $\omega_1^2 \in [1.67, 2.03]$ [s^{-2}] taking into account an uncertainty interval of ±5 % on the modal pulsation introduced by model parameter uncertainty, $\Omega^2 = 0.429$ [s^{-2}] $\rightarrow$ $\delta \in [3.89, 4.73]$ [] (see solid horizontal interval),
    - $|\Delta T_s| = 4934$ [N], $|\Delta T^*_{s,2n}| = 0.21$ [] $\rightarrow \epsilon = 0.12$ [].
- for $(V_0, N_v) = (4.25, N_v^1 - 1)$, which corresponds to a configuration without pumping:
    - $\omega_1^2 \in [1.67, 2.03]$ [s^{-2}] taking into account an uncertainty interval of ±5 % on the modal pulsation introduced by model parameter uncertainty, $\Omega^2 = 0.410$ [s^{-2}] $\rightarrow$ $\delta \in [4.07, 4.795]$ [] (see solid horizontal interval),
    - $|\Delta T_s| = 1725$ [N], $|\Delta T^*_{s,2n}| = 0.19$ [] $\rightarrow \epsilon = 0.05$ [].

The positioning of the chairlift's operating point in the stability diagram confirms that the configuration $(V_0, N_v) = (4.25, N_v^1)$ may be unstable, with amplification of the dynamic movement of the rope line as the system evolves with a steady state translation of vehicles, while the configuration $(V_0, N_v) = (4.25, N_v^1 - 1)$ is stable. When the vehicles move along the line, a parametric study shows that variations in modal pulsation are of the order of magnitude of $\Delta\omega_1 \approx 0.01\omega_1$ which modifies the δ of ±0.04. Indeed, Figure 14 shows that the operating point associated with

$(V_0, N_v) = (4.25, N_v^1)$ is likely to move into an unstable zone for a value of the damping coefficient $c_0 \in [0, 0.01]$.

Design application

The designer's aim is to stabilize the pumping dynamics observed for $(V_0, N_v) = (4.25, N_v^1)$. It has been seen that removing a vehicle, from N_v^1 to $N_v^1 - 1$, stabilizes the line but this is not necessarily the best solution as it reduces the passenger flow. Several parameters can be modified a posteriori when pumping is observed on an installation according to different strategies:

- By reducing the level of the excitation source through the cable speed V_0: the effect of a change in speed highlights the notion of critical speed or forbidden speed band that can be easily entered by the system's operator to avoid pumping.

  The boundary separating the stable from the instable zones is given by the following relation:

$$(n^2 - \delta)^2 = \epsilon^2 |T^*_{s,2n}|^2 - n^2 c_0^2. \tag{76}$$

  All other parameters being equal, as the cable speed V_0 changes, the excitation level ϵ remains equal while $\delta = \frac{\omega_1^2}{\Omega^2}$ varies with $\Omega = \frac{2\pi V_0}{l_d}$.

  In the configuration $(V_0, N_v) = (4.25, N_v^1)$, one can defined a forbidden speed band $V_{0,f} = [V_{0,f1}, V_{0,f2}]$ corresponding to the operating points inside the interval $[\delta_1, \delta_2]$ when the operating point is on or inside the boundary of instability:

$$\delta_1 = 4 - \sqrt{\epsilon^2 |T^*_{s,2n}|^2 - 4c_0^2}, \tag{77}$$

$$\delta_2 = 4 + \sqrt{\epsilon^2 |T^*_{s,2n}|^2 - 4c_0^2}, \tag{78}$$

  and by considering the variations in modal pulsation which modifies δ of ± 0.04. A numerical application yields $V_{0,f} = [4.19, 4.31]$ [m/s].
- With a control of the modal characteristics of the line $(\underline{\Phi}_k, \omega_k)$ by moving an intermediate support or modifying the level of mechanical tension controlled by Δ^2 parameter and

imposed on the cable loop by the counterweight or hydraulic actuator.

In general, support and cable tension modifications require heavy and invasive interventions on the installation, questioning its initial dimensioning. In another perspective of active damping of pumping instabilities, the role of the spectral content of tension evolution in triggering parametric resonance has been highlighted, opening the door to the study of a control-active system that would mechanically filter out harmful tension harmonics to escape system instabilities.

CONCLUSION AND PERSPECTIVES

This paper proposes an analysis of the pumping affecting single-cable transport lines by studying the cable tension signal as the system evolves over time. Pumping has long been known to occur in the ropeway industry but there is no analytical model for anticipating it in the design phase.

The analysis proposed in this paper is based on the case study of a chairlift that is subject to pumping, with tests carried out under real conditions for several configurations. The effect of a change in rope speed and vehicle spacing on the dynamic behaviour of the line is experimentally tested.

Based on the experimental data collected on the real system, a heuristic analysis of pumping reveals an internal excitation mechanism generated by the vehicles' travel, amplified by a geometric coincidence affecting the cable tension when two vehicles pass simultaneously over two support sheave assembly of the same span, which excites in a privileged way a mode of the cable line.

The analytical interpretation of pumping is based on the study of the Mathieu-Hill equation, which governs the dynamics of the system, under the effect of a parametric perturbation by the periodic tension evolution of the system. Parametric resonances correspond to zones of instability in which oscillations are amplified.

A numerical application highlights the pumping mode involved in chairlift line oscillations. The cable tension signal is calculated from the numerical model of the quasi-static evolution of the chairlift line as the vehicles move. The Fourier transform of the signal is used to extract the spectral content and shows the role of contact between the vehicle and the support in the excitation.

Finally, in the light of the results, possible approaches are proposed for defining optimal design parameter, in order to avoid system operating points likely to activate pumping.

Appendix 1: Reduced order model (ROM)

A reduced order model (ROM) is obtained using an inner product, defined on $\mathcal{H}_0([0,L])$ functions. The inner product is applied on the set of linear dynamic equations, expressed in the strong form Eq. (5), which involve a displacement $\underline{U}(S,t) = q(t)\underline{\Phi}_k(S)$ written as a linear combination of mode shape functions, and a test function which is evaluated as the mode shape unknown. This is an equivalent weak formulation of the problem given by Eq. (5) written in strong form, such as

$$\begin{aligned}
&\int_0^L (\Phi_{uk}^2 + \Phi_{vk}^2 + \Phi_{wk}^2)\mu \, \mathrm{d}S \, \ddot{q} \\
&\quad + \int_0^L \left[c_u \Phi_{uk}^2 \, \mathrm{d}S + c_v \Phi_{vk}^2 + c_w \Phi_{wk}^2 - 2\mu V_0 [\Phi'_{uk}\Phi_{uk} + \Phi'_{vk}\Phi_{vk} + \Phi'_{wk}\Phi_{wk}] \right] \mathrm{d}S \, \dot{q} \\
&+ \int_0^L \Bigg[\Phi_{uk}^2 \frac{T_s \kappa^2}{\|\underline{X}'\|} + \Phi_{vk}^2 \kappa^2 EA + \Phi_{uk}\Phi'_{vk} \left(\frac{T_s}{\|\underline{X}'\|} + EA \right) \kappa - \Phi_{vk}\Phi'_{uk} \left(\frac{T_s}{\|\underline{X}'\|} + EA \right) \kappa - \Phi_{uk}\Phi''_{uk} EA \\
&\qquad - \Phi_{vk}\Phi''_{vk} \frac{T_s}{\|\underline{X}'\|} - \Phi_{wk}\Phi''_{wk} \frac{T_s}{\|\underline{X}'\|} \\
&\quad + \mu V_0^2 [\Phi''_{uk}\Phi_{uk} + \Phi''_{vk}\Phi_{vk} + \Phi''_{wk}\Phi_{wk}] + \mu A_{V_0} [\Phi'_{uk}\Phi_{uk} + \Phi'_{vk}\Phi_{vk} + \Phi'_{wk}\Phi_{wk}] \Bigg] \mathrm{d}S \, q = 0. \quad (79)
\end{aligned}$$

The differential equation in time verified by the generalised coordinate q after projection onto the mode $\underline{\Phi}_k$ is that of a damped harmonic oscillator of ω_k pulsation according to the mode of vibration definition,

$$\ddot{q} + \Big(c_k + \Psi_k^1(V_0) \Big) \dot{q} + \Big(\omega_k^2 + \Psi_k^2(V_0, A_{V_0}) \Big) q = 0. \quad (80)$$

such as $\omega_k^2 = \dfrac{\int_0^L \left[\Phi_{uk}^2 \frac{T_s \kappa^2}{\|\underline{X}'\|} + \Phi_{vk}^2 \kappa^2 EA + \Phi_{uk}\Phi'_{vk} \left(\frac{T_s}{\|\underline{X}'\|} + EA \right) \kappa - \Phi_{vk}\Phi'_{uk} \left(\frac{T_s}{\|\underline{X}'\|} + EA \right) \kappa - \Phi_{uk}\Phi''_{uk} EA - \Phi_{vk}\Phi''_{vk} \frac{T_s}{\|\underline{X}'\|} - \Phi_{wk}\Phi''_{wk} \frac{T_s}{\|\underline{X}'\|} \right] \mathrm{d}S}{\int_0^L (\Phi_{uk}^2 + \Phi_{vk}^2 + \Phi_{wk}^2)\mu \, \mathrm{d}S}$,

$$\Psi_k^2(V_0, A_{V_0}) = \frac{\displaystyle\int_0^L \mu V_0^2[\Phi''_{uk}\Phi_{uk} + \Phi''_{vk}\Phi_{vk} + \Phi''_{wk}\Phi_{wk}] + \mu A_{V_0}[\Phi'_{uk}\Phi_{uk} + \Phi'_{vk}\Phi_{vk} + \Phi'_{wk}\Phi_{wk}]\ \mathrm{d}S}{\displaystyle\int_0^L (\Phi_{uk}^2 + \Phi_{vk}^2 + \Phi_{wk}^2)\mu\ \mathrm{d}S} \tag{81}$$

$$c_k = \frac{\displaystyle\int_0^L \left[c_u\Phi_{uk}^2\ \mathrm{d}S + c_v\Phi_{vk}^2 + c_w\Phi_{wk}^2\ \mathrm{d}S \right.}{\displaystyle\int_0^L (\Phi_{uk}^2 + \Phi_{vk}^2 + \Phi_{wk}^2)\mu\ \mathrm{d}S} \tag{82}$$

$$\Psi_k^1(V_0) = \frac{\displaystyle\int_0^L -2\mu V_0[\Phi'_{uk}\Phi_{uk} + \Phi'_{vk}\Phi_{vk} + \Phi'_{wk}\Phi_{wk}]\ \mathrm{d}S}{\displaystyle\int_0^L (\Phi_{uk}^2 + \Phi_{vk}^2 + \Phi_{wk}^2)\mu\ \mathrm{d}S} \tag{83}$$

Appendix 2: Multiple scale developments at order ϵ

At order ϵ, Eq. (40) is given by:

$$-2D_0D_1q_0 = -2D_1\left[Qj\sqrt{\delta}\ e^{j\sqrt{\delta}T_0} - \overline{Q}j\sqrt{\delta}\ e^{-j\sqrt{\delta}T_0}\right] = -2D_1Qj\sqrt{\delta}\ e^{j\sqrt{\delta}T_0} + 2D_1\overline{Q}j\sqrt{\delta}\ e^{-j\sqrt{\delta}T_0}, \tag{84}$$

$$-\left(\sum_{i>0} \Delta T_{s_i}^{*c}\cos(iT) + \Delta T_{s_i}^{*s}\sin(iT)\right) q_0 = -\left(\sum_{i>0} \Delta T_{s_i}^{*}\ e^{jiT_0} + \overline{\Delta T_{s_i}^{*}}\ e^{-jiT_0}\right)\left(Q\ e^{j\sqrt{\delta}T_0} + \overline{Q}\ e^{-j\sqrt{\delta}T_0}\right)$$

$$= -\sum_i \Delta T_{s_i}^{*}Q\ e^{j(i+\sqrt{\delta})T_0} + \Delta T_{s_i}^{*}\overline{Q}\ e^{j(i-\sqrt{\delta})T_0} + \overline{\Delta T}\,_{s_i}^{*}Q\ e^{j(-i+\sqrt{\delta})T_0} + \overline{\Delta T_{s_i}^{*}}\ \overline{Q}\ e^{j(-i-\sqrt{\delta})T_0}, \tag{85}$$

with $\Delta T_{s_i}^{*} = \frac{\Delta T_{s_i}^{*c} - j\Delta T_{s_i}^{*s}}{2}$

Appendix 3: Multiple scale development at order ϵ^2

By substituting q_0 et q_1 with their expressions given by developments at order ϵ^0 et ϵ:

$$-2D_0D_2q_0 = -2j\sqrt{\delta}D_2Q\ e^{j\sqrt{\delta}T_0} + 2j\sqrt{\delta}D_2\overline{Q}e^{-j\sqrt{\delta}T_0}, \tag{86}$$

$$-D_1^2q_0 = -D_1^2Q\ e^{j\sqrt{\delta}T_0} + cc. \tag{87}$$

The term $-2D_0D_1q_1$ is not resonant.

$$-\left(\sum_i T_{s_i}^*\, e^{jiT_0}+\overline{\Delta T_{s_i}^*}\, e^{-jiT_0}\right)q_1 = -\sum_m\sum_l \frac{\Delta T_{s_m}^*\Delta T_{s_l}^* Q}{l(l+2\sqrt{\delta})}\, e^{j(m+l+\sqrt{\delta})T_0} - \sum_m \sum_{\substack{l\\ l\neq 2n\\ l\neq m=n}} \frac{\Delta T_{s_m}^*\Delta T_{s_l}^* \overline{Q}}{l(l-2\sqrt{\delta})}\, e^{j(m+l-\sqrt{\delta})T_0}$$

$$-\frac{T_{s_n}^{*2}\overline{Q}}{n(n-2\sqrt{\delta})}\, e^{j2\epsilon\sigma T_0}e^{j\sqrt{\delta}T_0} - \sum_m \sum_{\substack{l\\ m-l\neq 2n}} \frac{\Delta T_{s_m}^*\overline{\Delta T_{s_l}^*}\,\overline{Q}}{l(l+2\sqrt{\delta})}\, e^{j(m-l-\sqrt{\delta})T_0} - \sum_m \sum_{\substack{l\\ m-l=2n}} \frac{\Delta T_{s_m}^*\overline{\Delta T_{s_l}^*}\,\overline{Q}}{l(l+2\sqrt{\delta})}\, e^{j2\epsilon\sigma T_0}e^{j\sqrt{\delta}T_0}$$

$$-\sum_m \sum_{\substack{l\\ l\neq 2n\\ l\neq m}} \frac{\Delta T_{s_m}^*\overline{\Delta T_{s_l}^*}Q}{l(l-2\sqrt{\delta})}\, e^{j(m-l+\sqrt{\delta})T_0} - \sum_{m\neq 2n} \frac{\Delta T_{s_m}^*\overline{\Delta T_{s_m}^*}Q}{m(m-2\sqrt{\delta})}\, e^{j\sqrt{\delta}T_0} - \sum_m\sum_{l\neq m} \frac{\overline{\Delta T_{s_m}^*}\Delta T_{s_l}^* Q}{l(l+2\sqrt{\delta})}\, e^{j(-m+l+\sqrt{\delta})T_0}$$

$$-\sum_m \frac{\overline{\Delta T_{s_m}^*}\Delta T_{s_m}^* Q}{m(m+2\sqrt{\delta})}\, e^{j\sqrt{\delta}T_0} - \sum_m \sum_{\substack{l\\ l\neq 2n\\ -m+l\neq 2n}} \frac{\overline{\Delta T_{s_m}^*}\Delta T_{s_l}^*\overline{Q}}{l(l-2\sqrt{\delta})}\, e^{j(-m+l-\sqrt{\delta})T_0} - \sum_m \sum_{\substack{l\neq 2n\\ -m+l=2n}} \frac{\overline{\Delta T_{s_m}^*}\Delta T_{s_l}^*\overline{Q}}{l(l-2\sqrt{\delta})}\, e^{j2\epsilon\sigma T_0}e^{j\sqrt{\delta}T_0}$$

$$-\sum_m\sum_l \frac{\overline{\Delta T_{s_m}^*}\;\overline{\Delta T_{s_l}^*}\;\overline{Q}}{l(l+2\sqrt{\delta})}\, e^{j(-m-l-\sqrt{\delta})T_0} - \sum_m\sum_{l\neq 2n} \frac{\overline{\Delta T_{s_m}^*}\;\overline{\Delta T_{s_l}^*}Q}{l(l-2\sqrt{\delta})}\, e^{j(-m-l+\sqrt{\delta})T_0}. \quad (88)$$

The secular terms of the equation in ϵ^2 are cancelled, i.e.:

$$-2j\sqrt{\delta}D_2Q - D_1^2Q - \frac{\Delta T_{s_n}^{*2}\overline{Q}}{n(n-2\sqrt{\delta})}\, e^{j2\epsilon\sigma T_0} - \sum_m \sum_{\substack{l\\ m-l=2n}} \frac{\Delta T_{s_m}^*\overline{\Delta T_{s_l}^*}\,\overline{Q}}{l(l+2\sqrt{\delta})}\, e^{j2\epsilon\sigma T_0}$$

$$-\sum_{m\neq 2n} \frac{\Delta T_{s_m}^*\overline{\Delta T_{s_m}^*}Q}{m(m-2\sqrt{\delta})} - \sum_m \frac{\Delta T_{s_m}^*\overline{\Delta T_{s_m}^*}Q}{m(m+2\sqrt{\delta})} - \sum_m \sum_{\substack{l\neq 2n\\ -m+l=2n}} \frac{\overline{\Delta T_{s_m}^*}\Delta T_{s_l}^*\overline{Q}}{l(l-2\sqrt{\delta})}\, e^{j2\epsilon\sigma T_0} = 0. \quad (89)$$

The expressions for D_1Q and D_1^2Q are given by the cancellation condition for secular terms in the ϵ order equation:

$$D_1Q = \frac{j}{2\sqrt{\delta}}\Delta T_{s_{2n}}^*\overline{Q}\, e^{j\sigma T_1}e^{j\sigma T_1}, \quad (90)$$

$$D_1^2Q = \left(\frac{j\Delta T_{s_{2n}}^*}{2\sqrt{\delta}}D_1\overline{Q} - \frac{\Delta T_{s_{2n}}^*\overline{Q}\sigma}{\sqrt{\delta}}\right) e^{j2\sigma T_1}, \quad (91)$$

$$D_1\overline{Q} = \frac{-j}{2\sqrt{\delta}}\overline{\Delta T_{s_{2n}}^*}Q\, e^{-j2\sigma T_1}. \quad (92)$$

By replacing,

$$D_1^2 Q = \frac{\overline{\Delta T_{s_{2n}}^*}\Delta T_{s_{2n}}^* Q}{4\delta} - \frac{\Delta T_{s_{2n}}^* \overline{Q}\sigma}{\sqrt{\delta}} e^{j2\sigma T_1}. \tag{93}$$

By injecting Eq. (93) into the cancellation condition for secular terms Eq. (89),

$$\begin{aligned} &-2j\sqrt{\delta}D_2 Q + \frac{\Delta T_{s_{2n}}^* \sigma \overline{Q}}{\sqrt{\delta}} e^{j2\sigma T_1} - \left(\sum_{m\neq 2n} \frac{\Delta T_{s_m}^* \overline{\Delta T_{s_m}^*}}{m(m-2\sqrt{\delta})} + \sum_m \frac{\Delta T_{s_m}^* \overline{\Delta T_{s_m}^*}}{m(m+2\sqrt{\delta})} + \frac{\Delta T_{s_{2n}}^* \overline{\Delta T_{s_{2n}}^*}}{4\delta} \right) Q \\ &- \left(\frac{\Delta T_{s_n}^{*2}}{n(n-2\sqrt{\delta})} + \sum_m \sum_{\substack{l \\ m-l=2n}} \frac{\Delta T_{s_m}^* \overline{\Delta T_{s_l}^*}}{l(l+2\sqrt{\delta})} + \sum_m \sum_{\substack{l \\ l\neq 2n \\ -m+l=2n}} \frac{\overline{\Delta T_{s_m}^*} \Delta T_{s_l}^*}{l(l-2\sqrt{\delta})} \right) \overline{Q} e^{j2\epsilon\sigma T_0} = 0. \end{aligned} \tag{94}$$

Appendixes 4: Non trivial solution conditions

Real and imaginary parts are separated,

$$\begin{cases} 2\sqrt{\delta}\ \frac{\mathrm{d}Q_I}{\mathrm{d}T} + 2\sqrt{\delta}Q_R\epsilon\sigma + \epsilon\big(-1+\frac{\epsilon\sigma}{\sqrt{\delta}}\big)|\Delta T_{s_{2n}}^*|Q_R - \epsilon^2(\Gamma_1 Q_R + \Gamma_{2R}Q_R + \Gamma_{2I}Q_I) &= 0, \\ 2\sqrt{\delta}\ \frac{\mathrm{d}Q_R}{\mathrm{d}T} - 2\sqrt{\delta}Q_I\epsilon\sigma + \epsilon\big(-1+\frac{\epsilon\sigma}{\sqrt{\delta}}\big)|\Delta T_{s_{2n}}^*|Q_I + \epsilon^2(\Gamma_1 Q_I + \Gamma_{2R}Q_I - \Gamma_{2I}Q_R) &= 0. \end{cases} \tag{95}$$

$$\begin{cases} 2\sqrt{\delta}\ \frac{\mathrm{d}Q_I}{\mathrm{d}T} + \Big[\epsilon\big[2\sqrt{\delta}\sigma + \big(-1+\frac{\epsilon\sigma}{\sqrt{\delta}}\big)|\Delta T_{s_{2n}}^*|\big] - \epsilon^2(\Gamma_1+\Gamma_{2R})\Big]\, Q_R - \epsilon^2\Gamma_{2I}Q_I &= 0, \\ 2\sqrt{\delta}\ \frac{\mathrm{d}Q_R}{\mathrm{d}T} + \Big[\epsilon\big[-2\sqrt{\delta}\sigma + \big(-1+\frac{\epsilon\sigma}{\sqrt{\delta}}\big)|\Delta T_{s_{2n}}^*|\big] + \epsilon^2(\Gamma_1+\Gamma_{2R})\Big]\, Q_I - \epsilon^2\Gamma_{2I}Q_R &= 0. \end{cases} \tag{96}$$

The system Eq. (96) admits solutions in the form $(Q_R, Q_I) = (q_R, q_I)\ e^{\gamma T}$, i.e. by replacing:

$$\begin{cases} (2\sqrt{\delta}\gamma - \epsilon^2\Gamma_{2I})q_I + \Big[\epsilon(-|\Delta T_{s_{2n}}^*| + 2\sqrt{\delta}\sigma) + \epsilon^2\big(\frac{\sigma|\Delta T_{s_{2n}}|}{\sqrt{\delta}} - \Gamma_1 - \Gamma_{2R}\big)\Big]\, q_R &= 0, \\ (2\sqrt{\delta}\gamma - \epsilon^2\Gamma_{2I})q_R + \Big[\epsilon(-|\Delta T_{s_{2n}}^*| - 2\sqrt{\delta}\sigma) + \epsilon^2\big(\frac{\sigma|\Delta T_{s_{2n}}|}{\sqrt{\delta}} + \Gamma_1 + \Gamma_{2R}\big)\Big]\, q_I &= 0. \end{cases} \tag{97}$$

Eq. (97) is written in the following matrix form,

$$\begin{bmatrix} \epsilon(-|\Delta T_{s_{2n}}^*| + 2\sqrt{\delta}\sigma) + \epsilon^2\big(\frac{\sigma|\Delta T_{s_{2n}}^*|}{\sqrt{\delta}} - \Gamma_1 - \Gamma_{2R}\big) & 2\sqrt{\delta}\gamma - \epsilon^2\Gamma_{2I} \\ 2\sqrt{\delta}\gamma - \epsilon^2\Gamma_{2I} & \epsilon(-|\Delta T_{s_{2n}}^*| - 2\sqrt{\delta}\sigma) + \epsilon^2\big(\frac{\sigma|\Delta T_{s_{2n}}^*|}{\sqrt{\delta}} + \Gamma_1 + \Gamma_{2R}\big) \end{bmatrix} \begin{pmatrix} q_R \\ q_I \end{pmatrix} = \begin{pmatrix} 0 \end{pmatrix}. \tag{98}$$

The existence of non-trivial solutions is ensured by canceling the determinant of the system matrix,

$$(2\sqrt{\delta}\gamma-\epsilon^2\Gamma_{2I})^2 = \epsilon^2\left[-|\Delta T_{s_{2n}}^*|+2\sqrt{\delta}\sigma+\frac{\epsilon\sigma|\Delta T_{s_{2n}}^*|}{\sqrt{\delta}}-\epsilon(\Gamma_1+\Gamma_{2R})\right]\left[-|\Delta T_{s_{2n}}^*|-2\sqrt{\delta}\sigma+\frac{\epsilon\sigma|\Delta T_{s_{2n}}^*|}{\sqrt{\delta}}+\epsilon(\Gamma_1+\Gamma_{2R})\right]. \tag{99}$$

Appendix 5: Case with damping

The resonant terms of order ϵ are now written:

$$-2D_1Qj\sqrt{\delta} - cQj\sqrt{\delta} - \Delta T_{s2n}\overline{Q}\ e^{j2\sigma T_1} = 0. \tag{100}$$

Similarly, the secular terms of order ϵ^2 can be written as:

$$\begin{aligned} &- 2j\sqrt{\delta}D_2Q - D_1^2Q - cD_1Q - \frac{\Delta T_{sn}^{*2}\overline{Q}}{n(n-2\sqrt{\delta})}\ e^{j2\epsilon\sigma T_0} - \sum_m \sum_{\substack{l \\ m-l=2n}} \frac{\Delta T_{sm}^*\overline{\Delta T_{sl}^*}\ \overline{Q}}{l(l+2\sqrt{\delta})}\ e^{j2\epsilon\sigma T_0} \\ &- \sum_{m\neq 2n} \frac{\Delta T_{sm}^*\overline{\Delta T_{sm}^*}Q}{m(m-2\sqrt{\delta})} - \sum_m \frac{\Delta T_{sm}^*\overline{\Delta T_{sm}^*}Q}{m(m+2\sqrt{\delta})} - \sum_m \sum_{\substack{l\neq 2n \\ -m+l=2n}} \frac{\overline{\Delta T_{sm}^*}\Delta T_{sl}^*\overline{Q}}{l(l-2\sqrt{\delta})}\ e^{j2\epsilon\sigma T_0} = 0. \end{aligned} \tag{101}$$

The expressions for D_1Q and D_1^2Q are given by the cancellation condition for secular terms in the ϵ order equation:

$$D_1Q = -\frac{cQ}{2} + \frac{j}{2\sqrt{\delta}}\Delta T_{s_{2n}}^*\overline{Q}\ e^{j2\sigma T_1}, \tag{102}$$

$$D_1\overline{Q} = -\frac{c\overline{Q}}{2} - \frac{j}{2\sqrt{\delta}}\overline{\Delta T_{s_{2n}}^*}Q\ e^{-2j\sigma T_1}, \tag{103}$$

$$D_1^2Q = \frac{c^2Q}{4} - \left(\frac{cj}{2\sqrt{\delta}} + \frac{\sigma}{\sqrt{\delta}}\right)\Delta T_{s_{2n}}^*\overline{Q}\ e^{j2\sigma T_1} + \frac{\Delta T_{s_{2n}}^*\overline{\Delta T_{s_{2n}}^*}Q}{4\delta}. \tag{104}$$

By injecting the expression for D_1^2Q into the cancellation condition for secular terms Eq. (101), one can obtain:

$$- 2j\sqrt{\delta}D_2Q - \frac{c^2Q}{2} + \left(\frac{cj}{2\sqrt{\delta}} + \frac{\sigma}{\sqrt{\delta}}\right)|\Delta T_{s_{2n}}^*|e^{j\phi_1}\overline{Q}e^{j2\sigma T_1}$$

$$-\frac{\Delta T_{s2n}^{*}\overline{\Delta T_{s2n}^{*}}Q}{4\delta}+\frac{c^2Q}{2}-\frac{cj}{2\sqrt{\delta}}\Delta T_{s2n}^{*}\overline{Q}e^{j2\sigma T_1}-|\Gamma_2|e^{j\phi_2}\overline{Q}e^{j2\sigma T_1}-\Gamma_1 Q=0. \quad (105)$$

The two cancellation conditions of the secular terms at orders ϵ and ϵ^2 given by Eq. (100) and Eq. (101) result from the development at different orders ϵ^n of:

$$-2j\sqrt{\delta}\,\frac{\mathrm{d}Q}{\mathrm{d}T}+\epsilon\left(-1+\frac{\epsilon\sigma}{\sqrt{\delta}}\right)\overline{Q}|\Delta T_{s2n}^{*}|e^{j(2\sigma\epsilon T+\phi_1)}-\epsilon cj\sqrt{\delta}Q-\epsilon^2\left[\left(\Gamma_1-\frac{c^2}{4}\right)Q+|\Gamma_2|\overline{Q}e^{j(2\epsilon\sigma T+\phi_2)}\right]=0. \quad (106)$$

Following the same approach as above, the cancellation condition for the exponent γ leads to the equation:

$$\epsilon^2|\Delta T_{s2n}^{*}|^2-4\delta\sigma^2\epsilon^2-\epsilon^4\left(\Gamma_1-\frac{c^2}{4}+\Gamma_{2R}\right)^2+\epsilon^4\Gamma_{2I}^2-\epsilon^2c^2\delta=0. \quad (107)$$

One can obtain:

$$\sigma^2=\frac{|\Delta T_{s2n}^{*}|^2-c^2\delta}{4\delta}+\frac{\epsilon^2}{4\delta}\left[\left(\Gamma_1-\frac{c^2}{4}+\Gamma_{2R}\right)^2+\Gamma_{2I}^2\right]. \quad (108)$$

Thus, the instability zones of the dynamic response of the cable transport line are given by:

$$\sigma>-\frac{\sqrt{|\Delta T_{s2n}^{*}|^2-c^2\delta}}{2\sqrt{\delta}}-\epsilon\frac{\sqrt{\left(\Gamma_1-\frac{c^2}{4}+\Gamma_{2R}\right)^2+\Gamma_{2I}^2}}{2\sqrt{\delta}}, \quad (109)$$

$$\sigma<\frac{\sqrt{|\Delta T_{s2n}^{*}|^2-c^2\delta}}{2\sqrt{\delta}}-\epsilon\frac{\sqrt{\left(\Gamma_1-\frac{c^2}{4}+\Gamma_{2R}\right)^2+\Gamma_{2I}^2}}{2\sqrt{\delta}}. \quad (110)$$

Data Availability Statement

Some or all data, models, or code generated or used during the study are proprietary or confidential in nature and may only be provided with restrictions

REFERENCES

Babaz, M. (2016). "Prédiction des instabilités dynamiques couplées aux non-linéarités dans les lignes de téléportés monocâbles." Ph.D. thesis, Centrale Lyon, Centrale Lyon.

Balmès, E., Ravary, F., and Langlais, D. (2004). "Uncertainty propagation in experimental modal analysis." *International Modal Analysis Conference*, United States (February).

Balmès, E. (2005). "Modes and regular shapes: how to extend component mode synthesis theory.." *Proceedings of the XI DINAME, 28th February-4th March 2005, Ouro Preto, MG, Brazil*.

Bécu, H., Lamarque, C.-H., and Ture Savadkoohi, A. (2023). "On the modal characteristics and stability of translating cable: Application to an overall line of cable transport systems." *Engineering Structures*, 292.

Bécu, H., Lamarque, C.-H., and Ture Savadkoohi, A. (2024). "Modal analysis of a time-variable ropeway system: Model reduction and vibration instability detection." *Topics in Modal Analysis & Parameter Identification, Volume 9*, B. J. Dilworth, T. Marinone, and M. Mains, eds., Cham, Springer Nature Switzerland, 133–144.

Berlioz, A. and Lamarque, C.-H. (2005). "A non-linear model for the dynamics of an inclined cable." *Journal of Sound and Vibration*, 279(3-5), 619–639.

Bertrand, C., Acary, V., Lamarque, C.-H., and Ture Savadkoohi, A. (2020). "A robust and efficient numerical finite element method for cables." *International Journal for Numerical Methods in Engineering*, 121(18), 4157–4186.

Bertrand, C., Ture Savadkoohi, A., Acary, V., and Lamarque, C.-H. (2022). "Reduced-order model for the non-linear dynamics of cables." *Journal of Engineering Mechanics - ASCE*, 148(9).

Brownjohn, J. (1998). "Dynamics of an aerial cableway system." *Engineering Structures*, 20, 826–836.

Crussels-Girona, M., Filippou, F., and Taylor, R. (2017). "A mixed formulation for nonlinear analysis of cable structures.." *Computers and Structures*, 186, 50–61.

Czitary, E. (1962). "Seilschwebahnen." *Springer-Verlag*.

Engel, E. and Löscher, R. (2005). "Zwei arten von pumpschwingungen." *Internationale Seilbahn-*

753 *Rundschau*, 6, 12–13.

754 Fei, H. and Danhui, D. (2020). "Free vibration of the complex cable system – an exact method
755 using symbolic computation." *Mechanical Systems and Signal Processing*, 139, 106636.

756 Fei, H., Zichen, D., and Danhui, D. (2020). "A novel method for dynamic analysis of complex
757 multi-segment cable systems." *Mechanical Systems and Signal Processing*, 142, 106780.

758 Hurel, G., Laborde, J., and Jézéquel, L. (2018). "Simulation of the dynamics behavior of a bi-cable
759 ropeway with modal bases." *In Topics in Modal Analysis Testing: Proceedings of the 36th IMAC,*
760 *A Conference and Exposition on Structural Dynamics*, Vol. 9, 43–54.

761 Irvine, H. (1992). *Cable structures.* Dover, New York.

762 Knawa-Hawryszków, M. (2017). "Influence of motion parameters on incidence of resonant track
763 rope vibrations in a bi-cable ropeway system." *Procedia Engineering X International Conference*
764 *on Structural Dynamics EURODYN 2017*, 2549–2554.

765 Lacarbonara, W. (2013). *Nonlinear Structural Mechanics, The Elastic Cable: From Formulation*
766 *to Computation*. Springer.

767 Luongo, A., Di Egidio, A., and Paolone, A. (2002). "On the proper form of the amplitude modula-
768 tion equations for resonant systems." *Nonlinear Dynamics*, 27, 237–254.

769 Löscher, R. (1997). "Pumpschwingungen bei einseilumlaufbahnen." Ph.D. thesis, Ph.D. thesis.

770 Marigo, J. (2014). "Mécanique des milieux continus, lecture notes." *École Polytechnique*.

771 Minorsky, N. (1945). "On parametric excitation." *Journal of the Franklin Institute*, 240, 25–26.

772 Nayfeh, A. and Mook, D. (1979). *Nonlinear oscillations*. John Wiley and Sons, New York.

773 Ntarladima, K. and Gerstmayr, J. (2023). "A multibody approach for the simulation of ropeway
774 systems." *ECCOMAS Thematic Conference on Multibody Dynamics, Lisbon, Portugal*.

775 Portier, B. (1984). "Dynamic phenomena in ropeways after a haul rope rupture." *Earthquake En-*
776 *gineering Structural Dynamics*, 12, 433–449.

777 Portier, B. (1985). "Rope oscillations in monocable ropeways." *Internationale Seilbahn-*
778 *Rundschau*, 3, 129–133.

779 Rega, G. (2004). "Nonlinear vibrations of suspended cables. part i: Modeling and analysis.." *Ap-*

780 *plied Mechanics Reviews*, 57, 443–475.
781 Renezeder, H. (2006). “On the dynamics of an axially moving cable with application to ropeways.”
782 Ph.D. thesis, Technische Universität Wien, Technische Universität Wien.
783 Renezeder, H. C., Steindl, A., and Troger, H. (2005). “On the dynamics of circulating monocable
784 aerial ropeways.” *Proceedings in Applied Mathematics and Mechanics*, 5, 123–124.
785 Renezeder, H. C., Steindl, A., and Troger, H. (2006). “Three-dimensional simulation of a circulating
786 monocable ropeway.” *Proceedings in Applied Mathematics and Mechanics*, 6, 327–328.
787 Saxon, D. and Cahn, A. (1953). “Modes of vibration of a suspended chain..” *The Quarterly Journal
788 of Mechanics and Applied Mathematics*, 6, 273–285.
789 Schneigert, Z. (1964). “Téléphériques et transporteurs aériens.” *Eyrolles*.
790 Xu, L., Hui, Y., Yang, Q., Chen, Z., and Law, S.-S. (2022). “Modeling and modal analysis of sus-
791 pension bridge based on continual formula method.” *Mechanical Systems and Signal Processing*,
792 162, 107855.

List of Tables

TABLE 1

Numerical data of the case study	
Cable length L	2236 m
Young's modulus E	130 GPa
Cable diameter d	45 mm
Cable linear mass μ	7.4 kg/m
Static tension Δ^2 parameter	1.9×10^5 N
Static curvature κ parameter	10^{-3} m^{-1}
Pulley radius R	3.05 m

TABLE 2

Vehicle number N_v [ ]	N_v^1			$N_v^1 - 1$		
Cable speed V_0 [m/s]	4.25	4.50	5.00	4.25	4.50	5.00
Line dynamic behavior [ ]						
Driving motor torque oscillation $\frac{C_{max}-C_{min}}{C_{moy}}$ [%]	120	51	40	19	x	x

TABLE 3

Vehicle number N_v [ ]	N_v^1			$N_v^1 - 1$		
Cable speed V_0 [m/s]	4.25	4.50	5.00	4.25	4.50	5.00
Spacing distance l_d [m]	42.0			42.7		
Fondamental excitation pulsation Ω_e [rad/s]	0.655	0.694	0.771	0.640	0.678	0.753

List of Figures

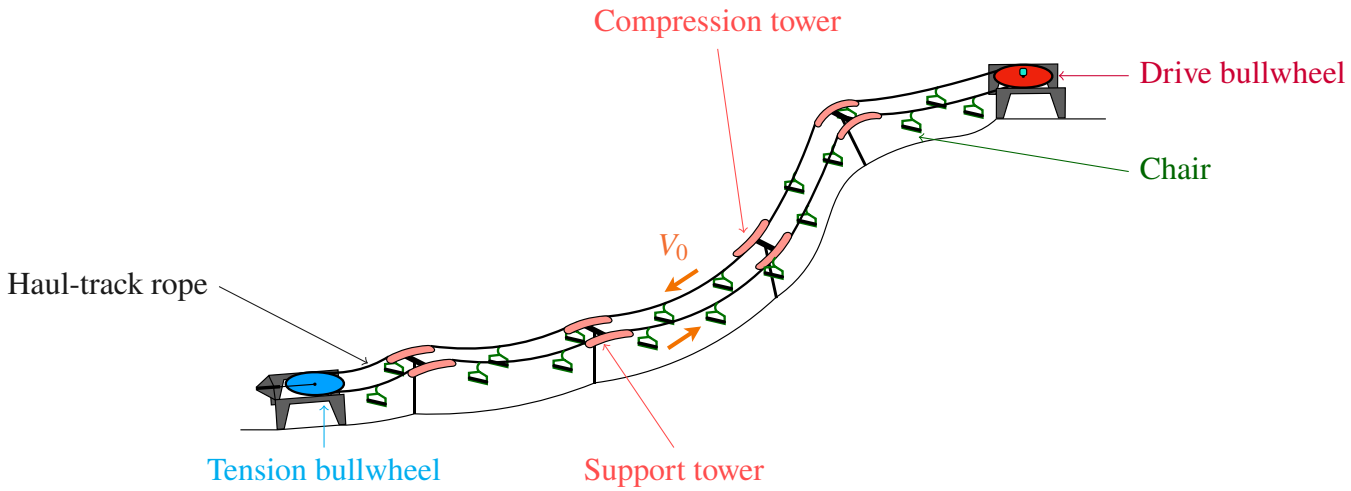

Fig. 1. Chairlift scheme

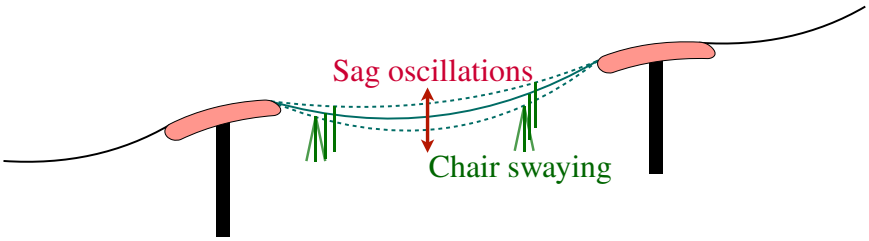

Fig. 2. Pumping scheme

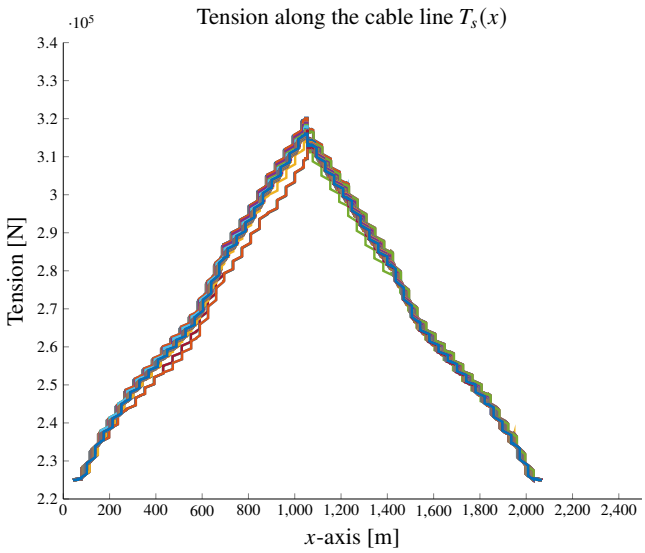

Fig. 3. Tension T_s along the cable line for several vehicle positions

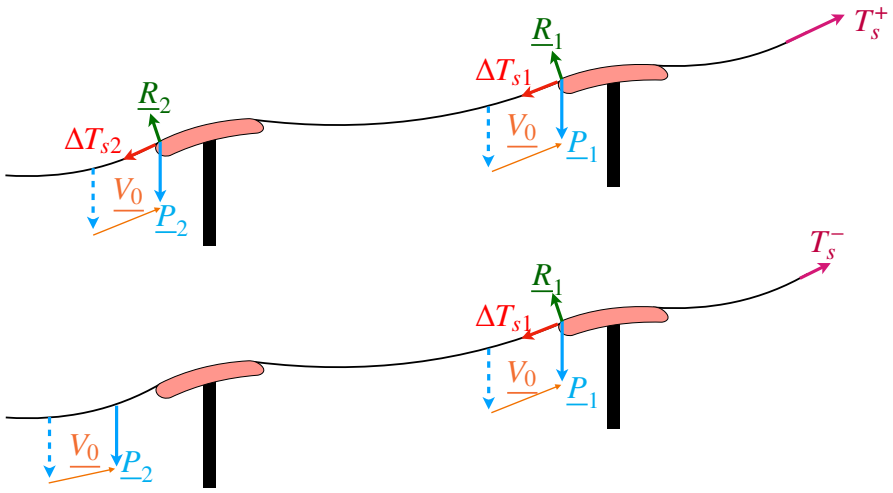

Fig. 4. Geometric cable span and vehicle spacing coincidence scheme

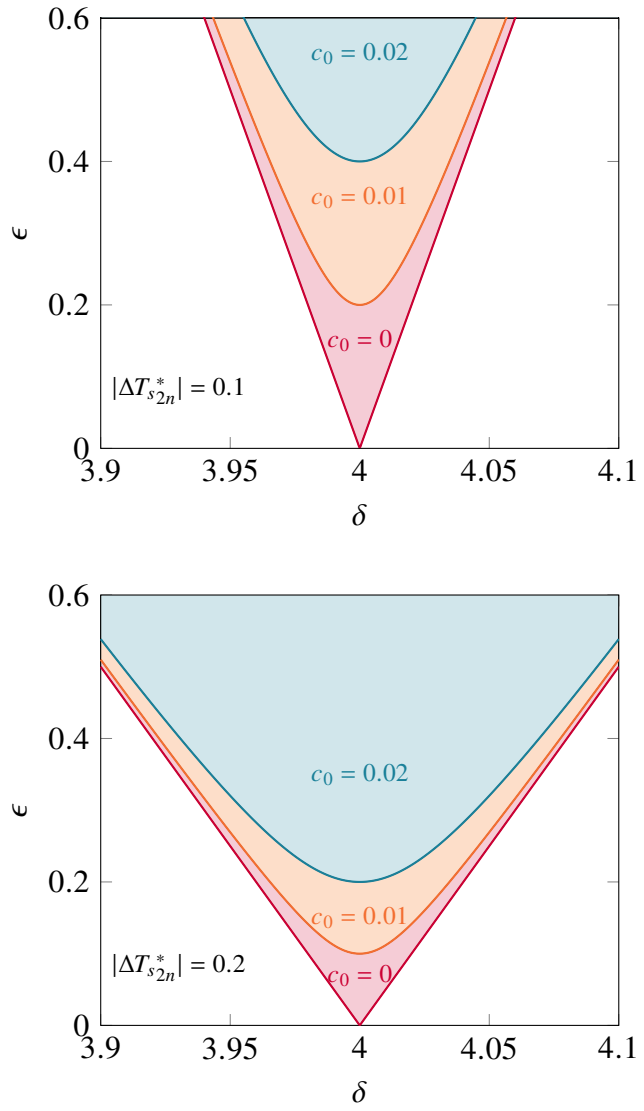

Fig. 5. Colored surfaces delimit areas of cable transport line instability (a) $|\Delta T^*_{s_{2n}}| = 0.1$, (b) $|\Delta T^*_{s_{2n}}| = 0.2$

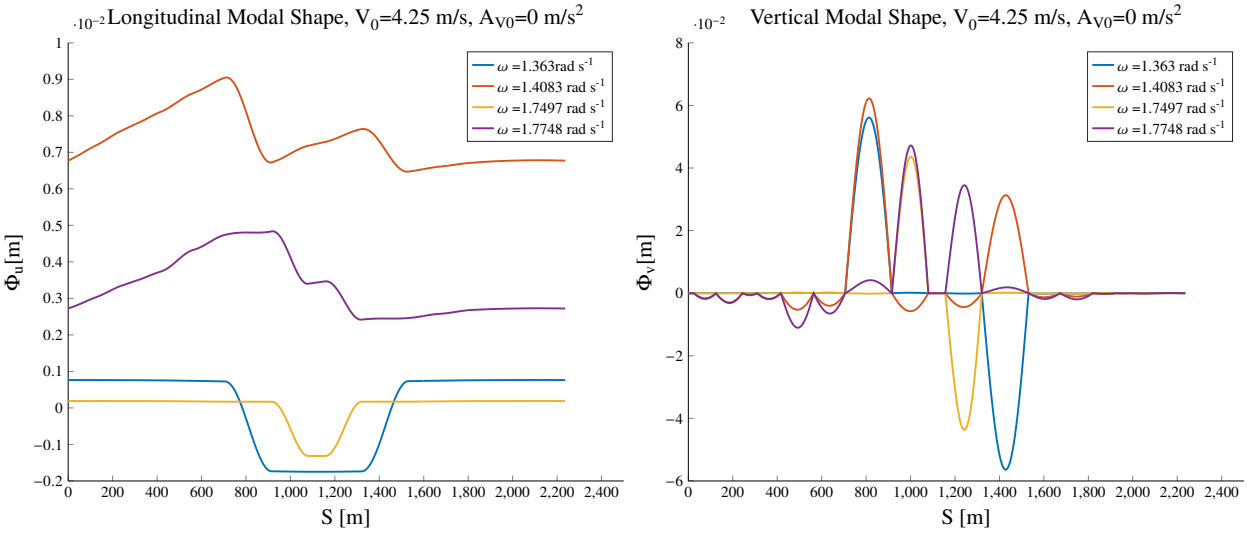

Fig. 6. First chairlift line (a) longitudinal and (b) vertical in-plane modes

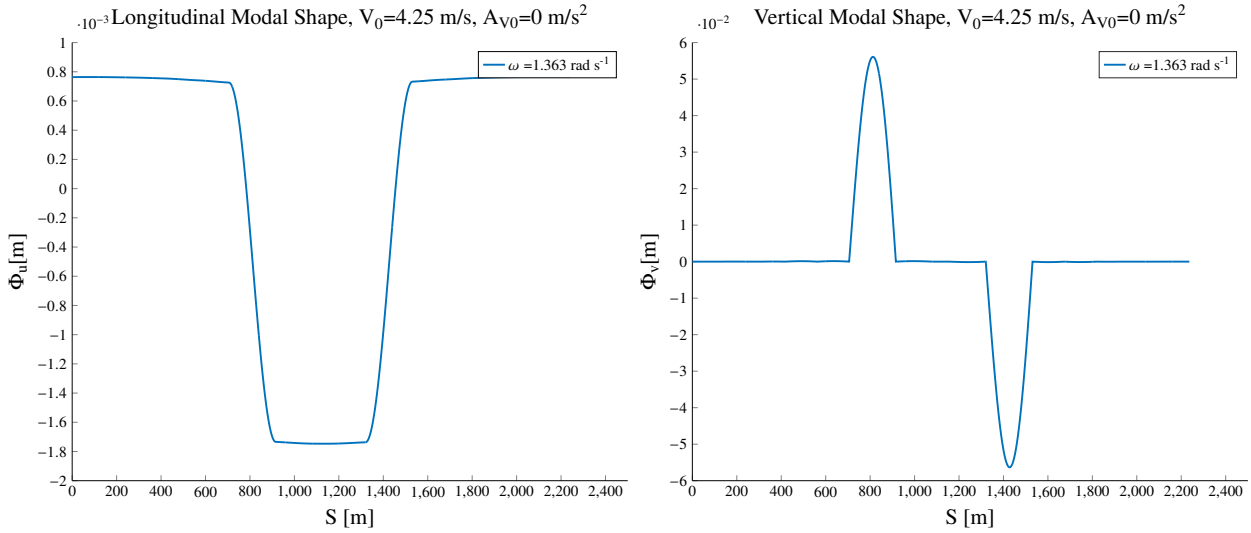

Fig. 7. Chairlift line (a) longitudinal and (b) vertical in-plane mode incriminated in pumping observation

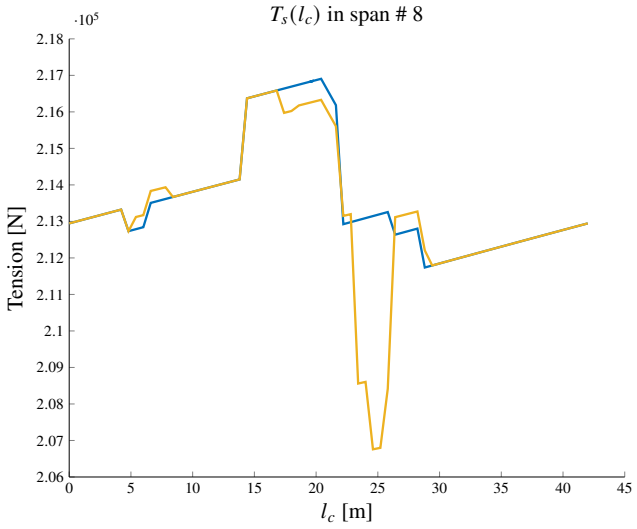

Fig. 8. Tension signal $T_s(l_c)$ in span # 8 for $(V_0, N_v) = (4.25, N_v^1)$ without (blue) and with (yellow) contact modelling between vehicle and tower's sheave assembly

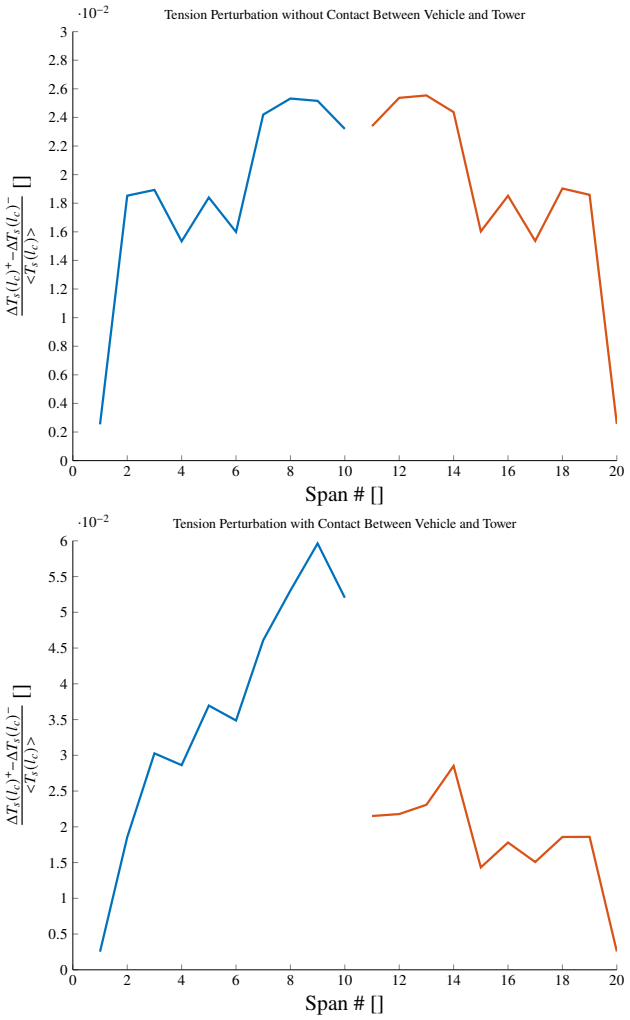

Fig. 9. Tension perturbation $\frac{\Delta T_s(l_c)^+ - \Delta T_s(l_c)^-}{<T_s(l_c)>}$ as function of the span number along the chairlift line for $(V_0, N_v) = (4.25, N_v^1)$ without (a) and with (b) contact modelling between vehicle and tower's sheave assembly

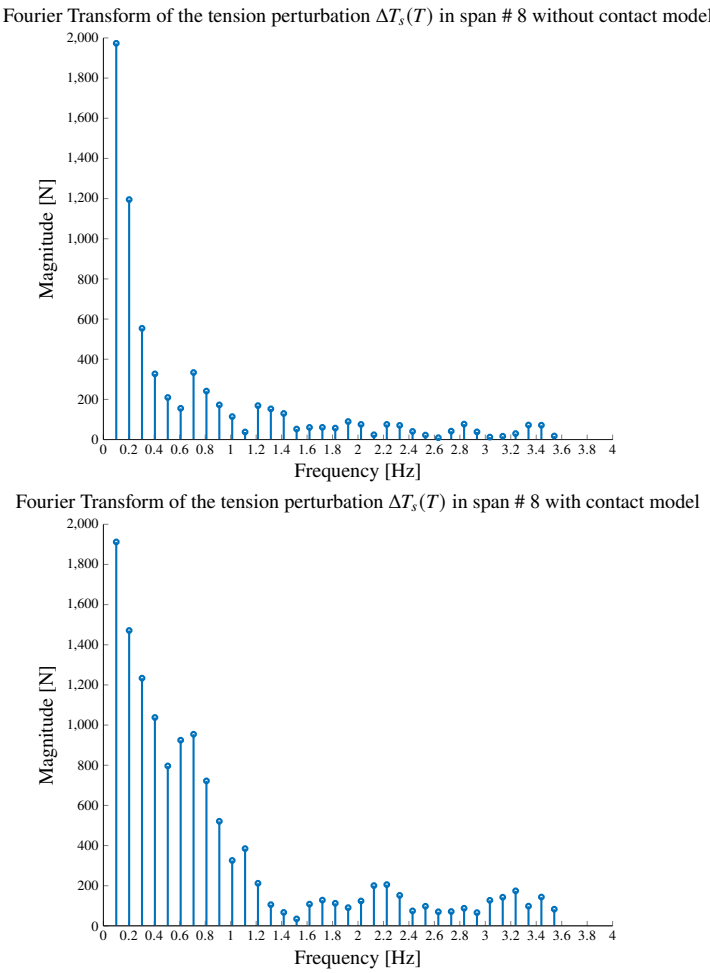

Fig. 10. Fast Fourier Transform of the tension $T_s(T)$ for $(V_0, N_v) = (4.25, N_v^1)$ without (a) and with (b) contact modelling between vehicle and tower's sheave assembly

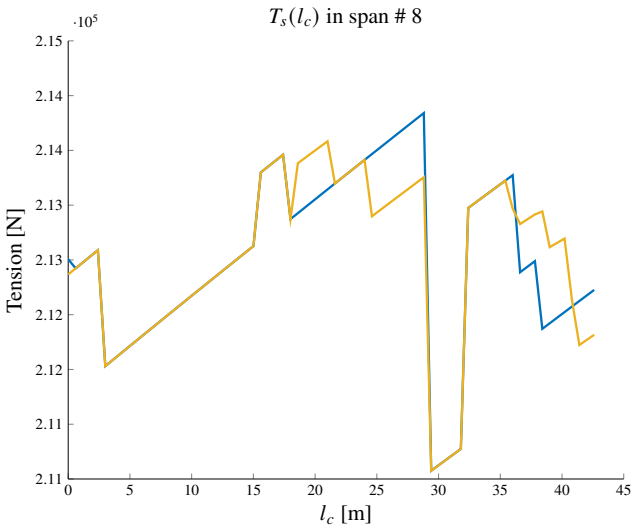

Fig. 11. Tension signal $T_s(l_c)$ in span # 8 for $(V_0, N_v) = (4.25, N_v^1 - 1)$ without (blue) and with (yellow) contact modelling between vehicle and tower's sheave assembly

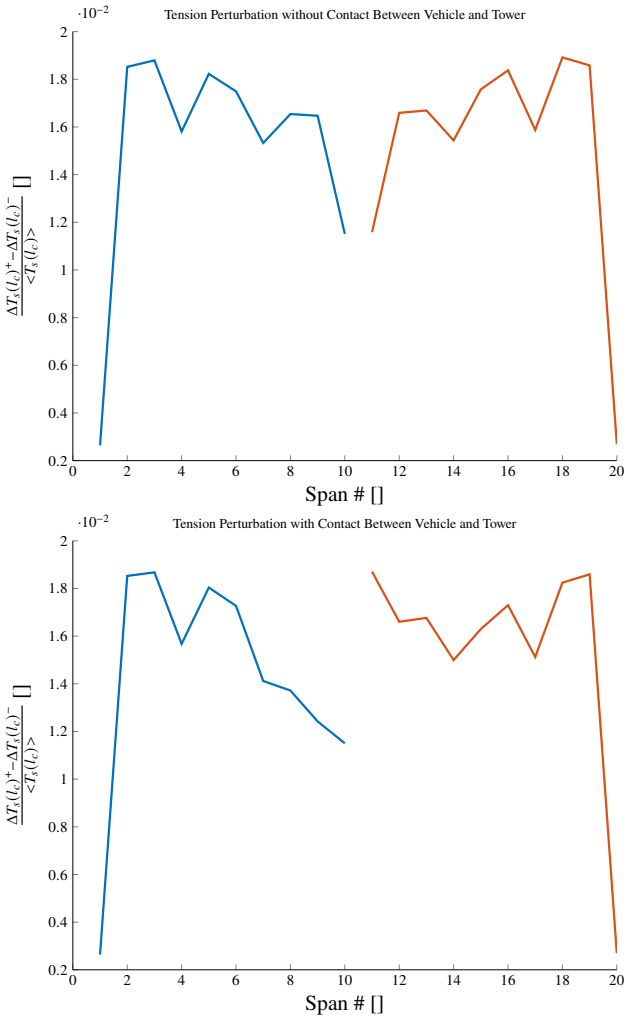

Fig. 12. Tension perturbation $\frac{\Delta T_s(l_c)^+ - \Delta T_s(l_c)^-}{<T_s(l_c)>}$ as function of the span number along the chairlift line for $(V_0, N_v) = (4.25, N_v^1 - 1)$ without (a) and with (b) contact modelling between vehicle and tower's sheave assembly

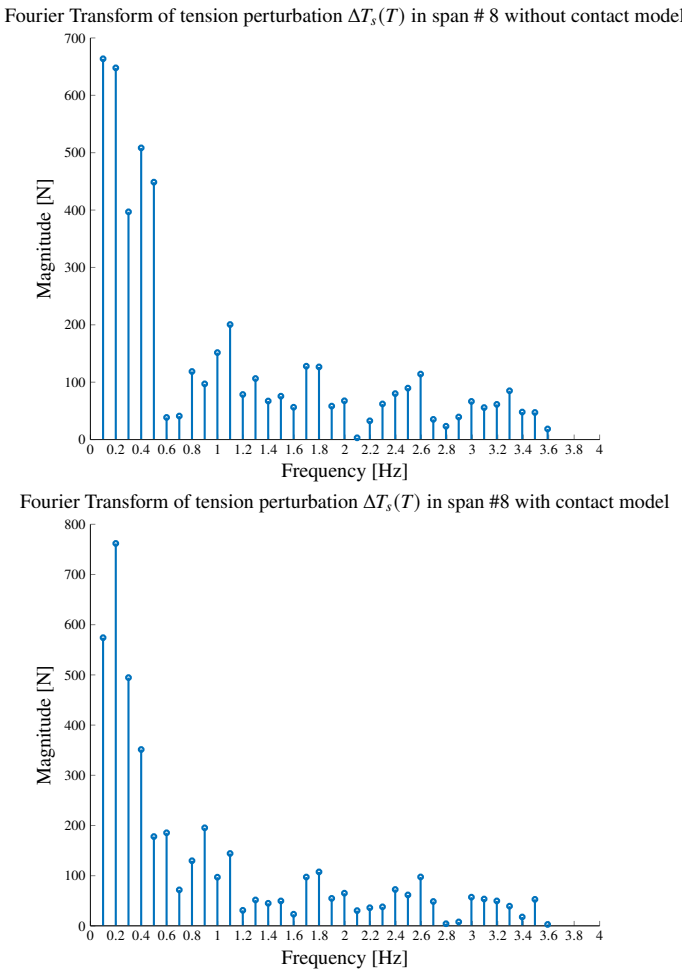

Fig. 13. Fast Fourier Transform of the tension $T_s(T)$ for $(V_0, N_v) = (4.25, N_v^1 - 1)$ without (a) and with (b) contact modelling between vehicle and tower's sheave assembly

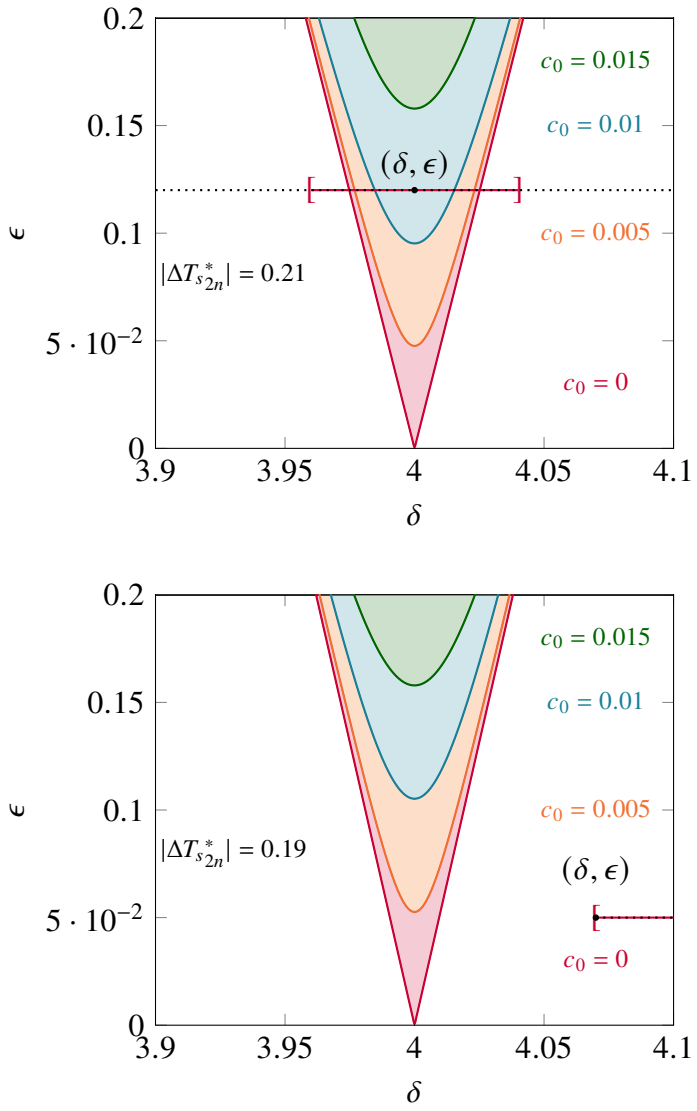

Fig. 14. Colored areas correspond to instable zones plotted according to (a) $|\Delta T^*_{s_{2n}}| = 0.19$, (b) $|\Delta T^*_{s_{2n}}| = 0.21$